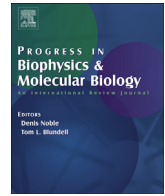




Contents lists available at ScienceDirect

Progress in Biophysics and Molecular Biology

journal homepage: www.elsevier.com/locate/pbiomolbio

Original Research

Accounting for cardiac t-tubule increase with age and myocyte volume to improve measurements of its membrane area and ionic current densities

Georges Christé ^{a, b, *}, Robert Bonvallet ^c, Christophe Chouabe ^d^a Laboratoire de Neurocardiologie, EA4612, Université Lyon 1, Lyon, F-69003, France^b INSERM, ADR Lyon, Lyon, F-69003, France^c CNRS UMR 5123, Campus de la Doua, Université Claude Bernard Lyon 1, 69622, Villeurbanne, France^d Université Lyon, CarMeN Laboratory, Institut National de la Santé et de la Recherche Médicale, Institut National de la Recherche Agronomique, Institut National des Sciences Appliquées de Lyon, Lyon, Université Claude Bernard Lyon 1, Bron, France

ARTICLE INFO

Article history:

Received 1 November 2019

Received in revised form

14 June 2020

Accepted 17 June 2020

Available online xxx

Keywords:

Cardiac myocytes

Rat

t-tubule

Volume

Capacitance

Morphology

Weight

Age

Model

ABSTRACT

In-silico models of cardiac myocytes allow simulating experiments in numbers on series of myocytes as well as on large populations of myocytes assembled in 3D structures. The simulated myocyte populations should have realistic values and statistical dispersions of biophysical parameters such as myocyte dimensions and volume and areas of the peripheral membrane and transverse-axial tubular system (TATS). Dependencies among these variables also have to be taken into account. In this work, we propose a quantitative representation of the changes in the fraction of membrane area in the TATS that integrates published dependencies with body weight (age) and size of rat ventricular cardiac myocytes while respecting the above constraints. Imposing a constant total membrane area-to-volume ratio appears to account for the increase of this fraction with myocyte size (i.e.: volume) within a given age group. The agreement of our results with published data was discussed and reasons for discrepancies were analysed. On the basis of our framework, strategies are proposed for minimizing the influence of non-random dispersion related to myocyte volume on measurements of the area of TATS and surface membrane compartments and of ionic current densities. The next step will be to quantitatively compare these strategies by evaluating the impact of myocyte morphological parameters and their dependencies, sample size, biases and errors, on the output of experiments.

© 2020 Elsevier Ltd. All rights reserved.

1. Introduction

It has early been recognized that the amount of transverse-axial tubular system (TATS) increased with age (Page and McCallister, 1973a; Nakamura et al., 1986) and with myocyte size (Leeson, 1978; Satoh et al., 1996). It also was seen that ventricular myocytes have large amounts of TATS whereas atrial myocytes generally have a lower amount (Leeson, 1978, 1980; Yue et al., 2017). In experimental rat models of cardiac hypertrophy (thyroid hormone), it was detected that myocytes have larger size and lower peripheral membrane area to myocyte volume ratio than in controls (McCallister and Page, 1973; Page and McCallister, 1973b). However, their total membrane area to

myocyte volume ratio was kept to control values, owing to the increase in the amount of TATS. The hypothesis was thus formulated that the purpose of the increase in TATS was to maintain a constant membrane area to myocyte volume ratio (McCallister and Page, 1973; Page and McCallister, 1973b). Owing to 3D reconstruction in confocal microscopy of living myocytes using a membrane-bound fluorescent marker, this idea was confirmed by the demonstration that the total membrane area increases in linear relation to myocyte volume (Satoh et al., 1996; Swift et al., 2006) in control rats. Indeed, the membrane area to myocyte volume ratio is a characteristic for a given species at a particular age (or body weight) and is maintained across differences in size of ventricular myocytes at that age (Satoh et al., 1996). In the present work, we simulate these changes and extend this simulation to younger ages (i.e.: lower body weights) to test whether the constraint of a constant area to volume ratio might reproduce the increase in the amount of TATS reported during development. Care

* Corresponding author. EA 4612 Neurocardiologie, Université Lyon 1, Faculté de Pharmacie de Lyon, 8, avenue Rockefeller, 69373, Lyon, Cedex 08, France.

E-mail address: christe.georges@laposte.net (G. Christé).

<https://doi.org/10.1016/j.pbiomolbio.2020.06.005>

0079-6107/© 2020 Elsevier Ltd. All rights reserved.

Abbreviations

AV-node	atrio-ventricular node
C_m	whole-cell membrane capacitance
di-8-ANEPPS	4-(2-[6-(Diocetyl amino)-2-naphthalenyl]ethenyl)-1-(3-sulfopropyl)pyridinium
f_{tres}	fraction of the TATS membrane that resisted detubulation
l	myocyte length
l_{mean}	average length
peri	perimeter of the cross-section of a myocyte
SA-node	sino-atrial node
SD_l	standard deviation of the length l
SD_{th}	standard deviation of the thickness th
SD_w	standard deviation of the width w

S_{end}	area of the end surface of a myocyte (~cross-sectional area)
S_{long}	area of the longitudinal surface of a myocyte
S_{surf}	area of the peripheral membrane of a myocyte
$S_{\text{surf}}/V_{\text{myo}}$	ratio of surface membrane area to myocyte volume
S_{tot}	total membrane area of a myocyte
$S_{\text{tot}}/V_{\text{myo}}$	ratio of total membrane area to myocyte volume
S_{tt}	membrane surface area of the TATS in a myocyte
$S_{\text{tt}}/S_{\text{tot}}$	ratio of TATS membrane area to total membrane area
$S_{\text{tt}}/V_{\text{myo}}$	ratio of TATS membrane area to myocyte volume
th	myocyte thickness
th_{mean}	average thickness
TATS	transverse-axial tubular system
V_{myo}	myocyte volume
w	myocyte width
w_{mean}	average width

was taken to incorporate the most detailed descriptions of the shape of ventricular myocytes. In particular, documented quantitative relationships among length, width and thickness of myocytes were taken into account, as well as the contribution of membrane infolding and caveolae and the most plausible estimate of the specific membrane capacitance value. Conflicting values in published accounts of the quantitative importance of TATS in ventricular cardiac myocytes of rats have been discussed (Soeller and Cannell, 1999; Pasek et al., 2008b). We review these papers critically and explore whether such differences might have been due to measurement artefacts and/or to using animals of different ages, hence of different body weights.

2. Methods

2.1. Softwares

All computations used in this work were written as scripts suited to both Matlab (The MathWorks, Natick, MA, USA) and Scilab (ESI Group, Rungis, France) further data processing and figures were prepared under Origin 7 (OriginLab Corporation, Northampton, MA, USA).

2.2. Rationale for building a synthetic set of data to represent changes in TATS with age or weight and myocyte size

The morphological model to represent a cardiac ventricular myocyte was chosen to be a rod with ellipsoid cross section. A synthetic data set was generated: several sizes were chosen to span the 95% confidence interval of width, length and depth as measured by Satoh et al. (1996). This was done for the two age groups i.e. 3 months (~350 g body weight) and 6 months (~500 g body weight) studied by Satoh et al. (1996), as described in the Appendix. Two additional data sets were generated by extrapolating myocyte sizes down to rat weights of 250 and 200 g (corresponding to younger rats). The two basic assumptions were that average myocyte size increased linearly with age (or body weight, see 4.5 Limitations), and that the relative dispersion of myocyte dimensions was the same as in the data of Satoh et al. (1996). In addition, a volume rendering factor was applied to convert the computed volume to rendered myocyte volume (Satoh et al., 1996).

The peripheral area and volume were computed for each myocyte size of the synthetic data set as indicated above and in the Appendix.

The peripheral area to volume ratio was computed. The whole-myocyte capacitance to volume ratio was set to the values reported

by Satoh et al. i.e.: 6.76 pF/pL for 3 months (~350 g) and 8.88 pF/pL for 6 months (~500 g) rats, and we assumed that the total capacitance to volume ratio at 3 months would also apply when extending our simulations to younger animals (250 and 200 g). Under the hypothesis that the extent of TATS membrane area would ensure that the total membrane area to volume ratio is maintained, the expected value of the fraction of membrane in the TATS was computed from those data.

Several corrections were applied to take into account the presence of peripheral membrane grooves, caveolae and of infolding of the membrane at the intercalated disk, which all increase the membrane area. Instead of the consensual value of $1 \mu\text{F}/\text{cm}^2$, a more realistic value of $0.9 \mu\text{F}/\text{cm}^2$ was used to translate membrane capacitance into area (see Appendix).

3. Results

3.1. A constrained design for artificial series of myocytes

We started with the assumptions that the myocytes were elongated rods with elliptic cross section and that myocyte width and thickness were linearly related to myocyte length. We created artificial datasets with lengths spanning the confidence interval around the mean length from published measurements for two average animal weights: 350 g (3 months) and 500 g (6 months). This was extrapolated down to two smaller average animal weights. We then computed the area of the peripheral myocyte membrane including corrections for membrane infolding, caveolae and intercalated disks. We also computed the myocyte volume and applied a volume-rendering factor proper to each average animal weight to adjust for indentations of the myocytes. The peripheral membrane area to myocyte volume ratio was then derived. Fig. 1A shows that it increases when myocyte volume decreases. The shape of the relationship is quite similar at all rat ages. This increase is a non-linear function of myocyte volume and shows a steeper increase at smaller volumes. The maximal value of the peripheral membrane area to myocyte volume ratio is at the smallest volume for the younger rat age (diamonds for the 200 g series in Fig. 1A) and amounts to $0.46 \mu\text{m}^2/\mu\text{m}^3$. A similar relationship was established for Sprague-Dawley rats $S_{\text{surf}}/V_{\text{myo}}$ ratio decreasing from $0.53 \mu\text{m}^2/\mu\text{m}^3$ for 44.5 g body weight down to about $0.30 \mu\text{m}^2/\mu\text{m}^3$ at 300 g (Stewart and Page, 1978). We also plotted the relations of myocyte volume to projected area (length * width) in Fig. 1B, showing that volume increases slightly more than projected area in all synthetic data

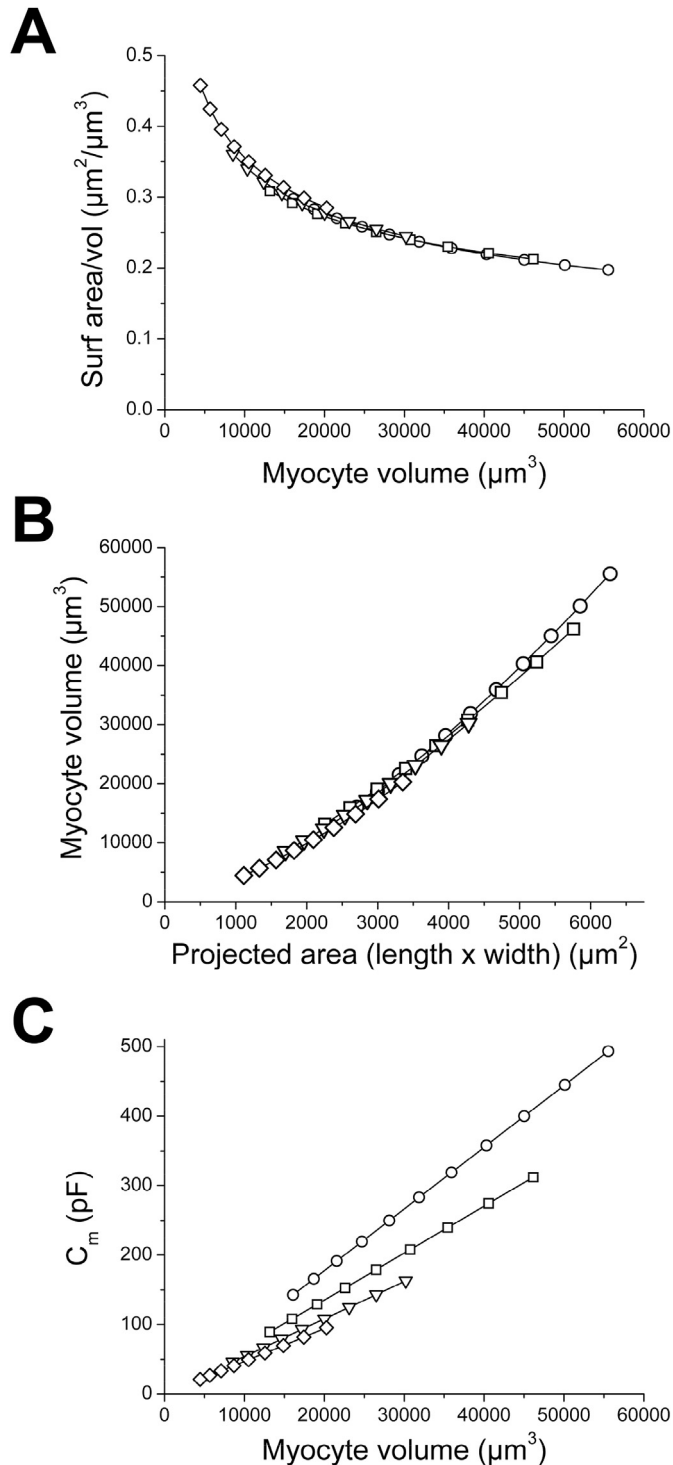


Fig. 1. Properties of the synthetic datasets representing ventricular myocytes in 6 months (~500 g, circles), 3 months (~350 g, squares) and younger rats (250 g, triangles and 200 g, diamonds). The symbols are connected by straight-line segments. **A:** Ratios of the peripheral area to myocyte volume S_{surf}/V_{myo} computed for the four series of synthetic data sets were plotted versus myocyte volume. **B:** The computed myocyte volumes were plotted versus the projected areas. **C:** The total myocyte capacitance values were plotted versus myocyte volume.

series. However when statistical errors would be added, the relation might be treated as linear as done in Fig. 4A of Satoh et al. (1996).

Knowing S_{surf}/V_{myo} and S_{tot}/V_{myo} , the ratio S_{tt}/V_{myo} was derived for each myocyte size in each series corresponding to different

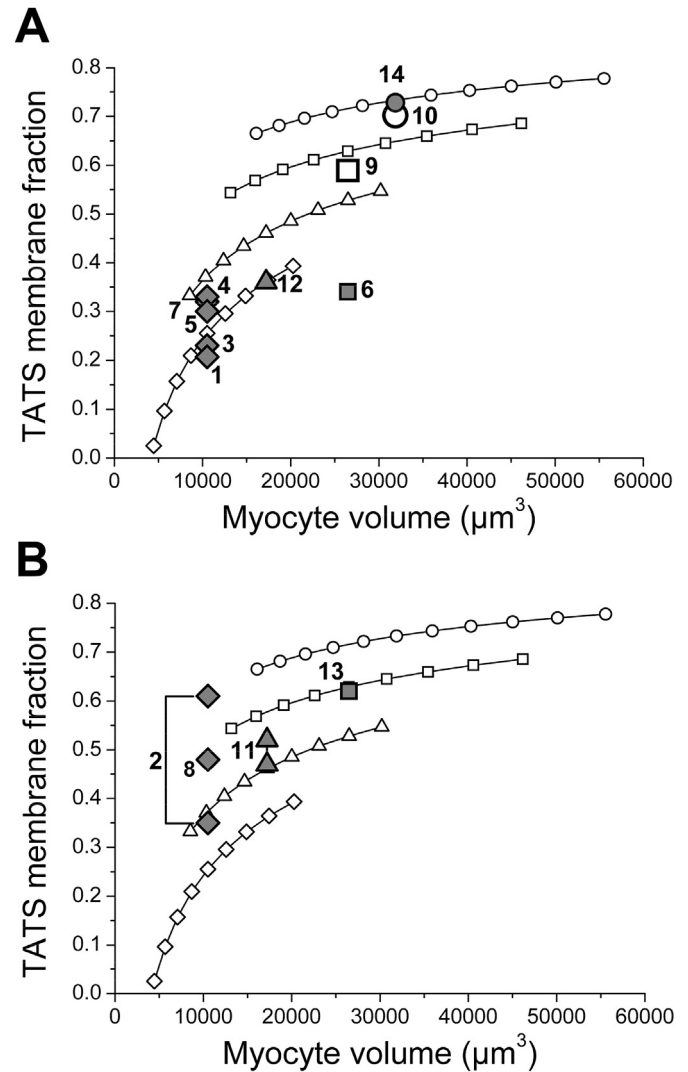


Fig. 2. Fraction of membrane area located in the TATS at different ages, plotted versus myocyte volume. Symbols of each synthetic data set are as in Fig. 1. The four graphs (open symbols plus line) are identical in panels A and B; they show the output of our simulations. Additional grey-filled symbols show data derived by stereological measurements from electron- or confocal-microscopy images (see Table 1 where the plotted data have been overshadowed in grey colour). The shape of the symbols is the same as the weight class of the corresponding rats. The numbers near the grey-filled and largest symbols refer to each study as indicated in the leftmost column of Table 1. In A, these symbols show data from Sprague-Dawley rats. The two largest symbols (labelled 9 and 10) refer to the TATS membrane fractions computed from the data of Satoh et al. (1996). In B, the filled symbols report measurements from Wistar rats. The two diamonds connected with a line labelled (2) are from data related to Payer (1971) in Table 1.

animal weights (or age). It was computed as the difference from S_{surf}/V_{myo} to the constrained S_{tot}/V_{myo} . Then, S_{tt}/S_{tot} was computed by dividing S_{tt}/V_{myo} by S_{tot}/V_{myo} (see in Appendix). As verification, whole myocyte C_m values were computed from the sum of S_{surf} and S_{tt} after conversion using a specific capacitance of $0.9 \mu\text{F}/\text{cm}^2$. Fig. 1C shows that our datasets respect the initial assumption of a constant C_m to V_{myo} ratio within a given age group.

The S_{tt}/S_{tot} data of all series are displayed in Fig. 2 (open symbols with line) versus myocyte volume and show that the values of S_{tt}/S_{tot} vary considerably with myocyte size within each age group, but also between groups with the age of the animals, and that this fraction increases steeply with myocyte size when starting from the smaller myocyte sizes. The increase with myocyte volume is relatively small

at later ages.

These graphs are duplicated in Fig. 2A and B and serve as a basis for comparing our simulation with values of the TATS membrane fraction that were derived from morphological studies, see 3.3 below.

3.2. Are published morphological estimates of the fraction of membrane in TATS in conflict?

The original data reported in various studies using morphological methods in electron microscopy or confocal microscopy have been collected in Table 1, and used to compute values of S_{tt}/S_{tot} , after applying corrections as explained in the Appendix.

We had to adjust our computations to the particular conditions of each study, which is detailed here below.

3.2.1. Satoh et al. (1996)

The peripheral membrane area for an ellipsoid cross section myocyte having average dimensions as in Table 2 of Satoh et al. was computed. Additionally, we took into account corrections for caveolae, membrane infolding and intercalated disk membrane

folding. We also computed the myocyte volumes from myocyte dimensions in Satoh et al.'s work, and, in order to match the average rendered volumes that they evaluated by 3D analysis for 3 months and 6 months rats, the rendering factor that we had to apply was 0.74 and 0.73 respectively. The values of S_{surf}/V_{myo} , computed from these estimates are $0.308 \mu\text{m}^2/\mu\text{m}^3$ for the 3 months rat and $0.295 \mu\text{m}^2/\mu\text{m}^3$ for the 6 months rat. This yields values of S_{tt}/S_{tot} of 0.544 and 0.668 respectively. The C_m/V_{myo} values of 6.76 and 8.88 pF/pL for 3 and 6 months respectively, were converted into S_{tot}/V_{myo} of $0.676 \mu\text{m}^2/\mu\text{m}^3$ and $0.888 \mu\text{m}^2/\mu\text{m}^3$ using a specific capacitance of $1 \mu\text{F}/\text{cm}^2$. When a specific capacitance value of $0.9 \mu\text{F}/\text{cm}^2$ was used, S_{tt}/S_{tot} was computed to 0.589 and 0.702 for 3 months and 6 months rats respectively.

3.2.2. Soeller and Cannell (1999).

They report a single S_{tt}/V_{myo} value of $0.44 \mu\text{m}^2/\mu\text{m}^3$. This value is the largest estimate of S_{tt}/V_{myo} (Table 1). Using a hypothetical myocyte of cylindrical shape $100 \mu\text{m}$ by $20 \mu\text{m}$, and the resulting volume of $31400 \mu\text{m}^3$, they estimated the ratio S_{tot}/V_{myo} to $6.6 \mu\text{m}^2/\mu\text{m}^3$, a value near to that reported by Satoh et al. (1996) for 3 months Sprague-Dawley rats weighting 350 g. Assuming a specific capacitance of

Table 1
Available quantitative morphological estimates describing the amount of TATS membrane area in rat myocytes.

	Strain	Age (weeks)/sex	Weight g	Method	C_m/n pF	V_{tt}/V_{myo} $\mu\text{m}^3/\mu\text{m}^3$	S_{surf}/V_{myo} $\mu\text{m}^2/\mu\text{m}^3$	S_{tot}/V_{myo} $\mu\text{m}^2/\mu\text{m}^3$	S_{tt}/V_{myo} $\mu\text{m}^2/\mu\text{m}^3$	S_{tt}/S_{tot}	3D-Rendering factor	
1	Page et al. (1971)	Sprague-Dawley	na/F	200	Stereology	na	0.012	0.27	0.34	0.07	0.207	
2	Pager (1971)	Wistar	Adult/na	200	Stereology EM	na	0.0106	0.33 ^c	0.41 ^c	0.0847 ^c	0.207	
								0.44*	0.25	0.57		
								0.49**	0.30^c	0.61		
								0.76*	0.30^c	0.39		
								0.84**	0.30^c	0.35		
3	Page and McCallister (1973a)	Normal rat	na/na	200	Stereology	na	0.01	0.3	0.39	0.09	0.23	
4	Page (1978) ^a	Rat	na/na	na	Stereology EM	na		0.36 ^c	0.47 ^c	0.109 ^c	0.23	
											0.33	
5	Stewart and Page (1978)	Sprague-Dawley	na/F	222	Stereology EM	na	0.004	0.3	0.43	0.13	0.30	
6	Stewart and Page (1978)	Sprague-Dawley	na/F	300	Stereology EM	na	0.008	0.3	0.47	0.16	0.34	
7	Page and Surdyk-Droske (1979)	Sprague-Dawley	na/F	200–260	Stereology	na	na	0.307	0.457	0.145	0.32	
	Nakamura et al. (1986)	Wistar	7/FM	200	Stereology EM	na	0.0075	0.371 ^c	0.553 ^c	0.175 ^c	0.32	
								0.676*	0.30	0.44		
									0.363 ^c	0.48		
9	Satoh et al. (1996)	Sprague-Dawley	3 months	346 (330–378)	Confocal 3D	207 ± 8.3/14	na	0.308 ^{c d}	0.676*	0.368*	0.544	0.74
10	Satoh et al. (1996)	Sprague-Dawley	6 months	496 (480–516)	Confocal 3D	324 ± 14/14	na	0.295 ^{c d}	0.75**	0.442**	0.589	0.73
									0.888*	0.593*	0.668	
									0.99**	0.695**	0.702	
11	Soeller and Cannell (1999)	Wistar	na/na	250	Confocal 3D	na	0.036	0.676*	0.44	0.65	0.71	
									0.75**	0.44	0.59	
									0.843*	0.44	0.52	
									0.94**	0.44	0.47	
									0.76*	0.44	0.58	
									0.84**	0.44	0.52	
12	Despa et al. (2003)	Sprague-Dawley	11 ⁴ /M	~300	Confocal 3D	156 ± 7/24	na	0.373 ^{c d}	0.51*		0.27	
13	Swift et al. (2006)	Wistar	na/M	300	Confocal 3D	199 ± 9/9	na	0.361 ^{c d}	0.57**		0.36	
									0.843*		0.57	
									0.94**		0.62	
14	Gorelik et al. (2006)	Sprague-Dawley	Adult/M	490	Confocal 3D	na	na	na			0.728	
											0.432^b	

In bold: values measured by the authors. In italics: values computed from their data (see section 3.2). na: not available. * and **: computed from authors' data, assuming a specific capacitance of * $1 \mu\text{F}/\text{cm}^2$ or ** $0.9 \mu\text{F}/\text{cm}^2$.

² This is the ratio of di-8-ANEPPS fluorescence in the TATS (whole confocal slice image minus peripheral membrane) to fluorescence from the whole confocal slice. See section 3.2 for further discussion.

⁴ Age derived from breeder's data in Pasek et al., (2017).

^a Quoted by (Yao et al., 1997) and (Satoh et al., 1996).

^b The same ratio in detubulated myocytes.

^c Corrected for area of caveolae.

^d Corrected for membrane infolding.

Table 2Values of changes in membrane capacitance upon formamide detubulation of adult rat ventricular myocytes. Values are mean \pm sem with the number of myocytes n.

Ref	Animal/strain	Weight (g)/Age (week)	C _m eval. method	C _m control (pF)/n	C _m detubul. (pF)/n	% C _m lost/ f _{tres}	C _m /V _{myo} (pF/pL)	% C _m lost corr.	V _{myo} (pL)
Kawai et al. (1999)	Adult female Wistar	na	na	199.4 \pm 19/13	146.7 \pm 6.4/13	26.6		32.2	
Komukai et al. (2002)	Adult male Wistar	250	na	200 \pm 7/37	160 \pm 8/23	20.0		24.4	
Yang et al. (2002)	Adult male Wistar	~250/7 ^h	na	193 \pm 41/25	143 \pm 34/25	25.9/0.08		31.6	
Despa et al. (2003)	Male Sprague-Dawley	~300/11 ^h	na	156 \pm 7/24	106 \pm 5/19	32.1/0.08		39.1	
Thomas et al. (2003)	Male Wistar	~300/9 ^h	Integration	204 \pm 11/23	150 \pm 7/13	26.5/0		32.3	
Brette et al. (2004a)	Male Wistar	na	na	193 \pm 22/22	137 \pm 34/22	29.0		35.4	
Brette et al. (2004b)	Male Wistar	na	Integration	178 \pm 11/11	132 \pm 3/10	25.8		31.5	
Duclohier (2005)	Adult male Sprague Dawley ^a	na	na	135 \pm 7/13	105 \pm 9/na	22.2		27.1	
Brette et al. (2006)	Male Wistar	250–300	Integration	186 \pm 11/14	133 \pm 8/13	28.5		34.7	
Swift et al. (2006)	Male Wistar	~300	Integration	199 \pm 9/9	140 \pm 14/7	29.6/0.08 ^f	8.4	36.2	23.6
Brette and Orchard (2006a)	Male Wistar	na	na	156 \pm 9/14	115 \pm 5/17	26.3		32.1	
Brette and Orchard (2006b)	Male Wistar	na	na	174 \pm 9/24	120 \pm 5/25	31.0		37.8	
Despa and Bers (2007)	Rat	na	na	164 \pm 6/12	120 \pm 8/9	27.0		32.7	
Swift et al. (2007)	Male Wistar	~300/~10	Integration	235 \pm 7.8/11	178 \pm 7/11	24.3/0.08 ^f	7.6	29.6	30.8
Swift et al. (2008)	Male Wistar	~300/~10	Integration	237 \pm 15/11	181 \pm 6/11	23.6/0.08 ^f		28.8	
Chase et al. (2010) ^f	Male Wistar	na	na	207.3 \pm 11.0/13	144.7 \pm 5.5/18	30.2		36.8	
Garciaarena et al. (2013) ^e	Adult male Sprague Dawley	300/11 ^h	Integration	236 \pm 26/9	139 \pm 14/8	41.0	14.4	50.1	16.4
Bryant et al. (2014)	Adult male Wistar	250–300	na	283 \pm 22/11	167 \pm 11/11	41/		50.0	
Bryant et al. (2015)	Adult male Wistar ^b	~460/~25	na	260 \pm 9/37	178 \pm 9/28	31.5		38.5	
Gadeberg et al. (2016)	Male Wistar	~460/~25	na	240.2 \pm 21/12	206.2 \pm 11/9 ^g	14.2/0.16		–	
Bourcier et al. (2019)	Male Wistar	250–300	na	184.2 \pm 10.8/21 ^c	105.2 \pm 6.4/21 ^c	40.6 ^d (43.0)		52.3	
Mean values				201 \pm 8	143 \pm 6	28.5 \pm 1.5		35.7 \pm 1.7	

^a Isolated myocytes obtained from Harding SE's lab, who worked with Adult male Sprague Dawley rats (Lewis et al., 2004).^b 18 weeks after sham coronary artery ligation operation.^c The sem was computed from original SD.^d Original value at 43% was corrected for 6% incomplete detubulation to match conditions of formamide detubulation in other studies.^e Data was read from their Fig. 2B.^f Detubulation incomplete as discussed by authors.^g Detubulated data in control rat as indicated in Pasek et al. (2017).^h Age derived from the growth chart at <http://www.criver.com/by> Pasek et al. (2017).

1 $\mu\text{F}/\text{cm}^2$ they estimated the $S_{\text{tt}}/V_{\text{myo}}$ to 0.68. This was when assuming $S_{\text{tot}}/V_{\text{myo}}$ at $0.676 \mu\text{m}^2/\mu\text{m}^3$, as for 350 g male Sprague-Dawley rats. Assuming in turn the ratio $S_{\text{tot}}/V_{\text{myo}}$ to be 0.843 or $0.76 \mu\text{m}^2/\mu\text{m}^3$, as derived from Swift et al. (2007) and Swift et al. (2006) respectively, for 300 g male Wistar rats, would yield an $S_{\text{tt}}/S_{\text{tot}}$ value of 0.52 or 0.58. Soeller and Cannell (1999) used 250 g male Wistar rats, thus the $S_{\text{tt}}/S_{\text{tot}}$ of 0.52 may be considered as a lower limit and the value of 0.58 as an upper limit. These values changed to 0.47 and 0.52 respectively when considering a specific capacitance of $0.9 \mu\text{F}/\text{cm}^2$. It is surprising that Soeller and Cannell did not estimate S_{surf} and V_{myo} , which would have readily allowed estimation of $S_{\text{tt}}/S_{\text{tot}}$.

3.2.3. Swift et al. (2006).

A ratio of mean myocyte C_m to mean V_{myo} of 8.43 pF/pL was computed from their data. Assuming a specific capacitance of $0.9 \mu\text{F}/\text{cm}^2$, this is converted to a $S_{\text{tot}}/V_{\text{myo}}$ of $0.94 \mu\text{m}^2/\mu\text{m}^3$. The $S_{\text{surf}}/V_{\text{myo}}$ computed from the data in Satoh et al. (1996) for a myocyte of 200 pF capacitance (the mean value reported in Swift et al. (2006)) with an elliptical cross section amounts to $0.361 \mu\text{m}^2/\mu\text{m}^3$. Thus the $S_{\text{tt}}/S_{\text{tot}}$ may be estimated to 0.62. It would be 0.57 with a specific capacitance of $1 \mu\text{F}/\text{cm}^2$.

3.2.4. Page et al. (1971).

The authors reported, in 200 g Sprague-Dawley rats, an $S_{\text{surf}}/V_{\text{myo}}$ of $0.27 \mu\text{m}^2/\mu\text{m}^3$ and a $S_{\text{tot}}/V_{\text{myo}}$ of $0.34 \mu\text{m}^2/\mu\text{m}^3$. A direct calculation leads to an estimated $S_{\text{tt}}/S_{\text{tot}}$ of 0.207. Assuming that peripheral membrane infolding was duly taken into account in the stereological measurements and that caveolae were likely neglected, both ratios should be corrected for the presence of caveolae. In this case, as we

assumed the caveolae to increase membrane area by the same factor in peripheral and in TATS membrane, such correction would not change the computed $S_{\text{tt}}/S_{\text{tot}}$.

3.2.5. Pager (1971).

Jeanne Pager used 200 g Wistar rats. The reported value of $0.25 \mu\text{m}^2/\mu\text{m}^3$ for $S_{\text{tt}}/V_{\text{myo}}$ may be combined with an estimated $S_{\text{tot}}/V_{\text{myo}}$ of $0.44 \mu\text{m}^2/\mu\text{m}^3$, as evaluated by Swift et al. (2006) in 300 g male Wistar rats. In this case the $S_{\text{tt}}/S_{\text{tot}}$ would be 0.57. If now using a value of $0.9 \mu\text{F}/\text{cm}^2$ and in addition, correcting S_{tt} for caveolae, a value of 0.61 is computed. Lastly, using a $S_{\text{tot}}/V_{\text{myo}}$ of $0.76 \mu\text{m}^2/\mu\text{m}^3$ (computed assuming a specific capacitance of $1 \mu\text{F}/\text{cm}^2$ from Swift et al.'s (2007) C_m/V_{myo} estimate of 7.6 pF/pL) and correcting S_{tt} for caveolae a new value of $S_{\text{tt}}/S_{\text{tot}}$ of 0.39 is estimated, that is changed to 0.35 when considering $0.9 \mu\text{F}/\text{cm}^2$.

3.2.6. Page and McCallister (1973a).

From their measurements of $0.30 \mu\text{m}^2/\mu\text{m}^3$ and $0.39 \mu\text{m}^2/\mu\text{m}^3$ for respectively $S_{\text{surf}}/V_{\text{myo}}$ and $S_{\text{tot}}/V_{\text{myo}}$, the $S_{\text{tt}}/S_{\text{tot}}$ may be estimated to 0.23. As for the data of Page et al. (1971), correcting for caveolae would not alter the final computed $S_{\text{tt}}/S_{\text{tot}}$.

3.2.7. Page and Surdyk-Droske (1979).

Their estimates of $0.307 \mu\text{m}^2/\mu\text{m}^3$ for $S_{\text{surf}}/V_{\text{myo}}$ and $0.145 \mu\text{m}^2/\mu\text{m}^3$ for $S_{\text{tt}}/V_{\text{myo}}$ allow computing $0.457 \mu\text{m}^2/\mu\text{m}^3$ for $S_{\text{tot}}/V_{\text{myo}}$ and 0.32 for $S_{\text{tt}}/S_{\text{tot}}$. As was done above for the data of Page et al. (1971) and Page and McCallister (1973a), it may be assumed that infolding of the peripheral membrane has been taken into account, so that correcting $S_{\text{surf}}/V_{\text{myo}}$ and $S_{\text{tt}}/V_{\text{myo}}$ for caveolae did not change the

S_{tt}/S_{tot} that remained to 0.32.

3.2.8. Nakamura et al. (1986).

The same reasoning was applied to computations from the data of Nakamura et al. as from those of Pager (1971). The final estimates of S_{tt}/S_{tot} were 0.44 and 0.48 for a specific capacitance at 1 and 0.9 $\mu\text{F}/\text{cm}^2$ respectively.

3.2.9. Gorelik et al. (2006).

They used fluorescence intensity measurements of the membrane probe di-8-ANEPPS on isolated living rat cardiomyocytes and computed the ratio of fluorescence intensity in a confocal slice of a myocyte, excluding the peripheral membrane, to the total fluorescence intensity within the same slice. Although they designated this ratio the “volume ratio” of the TATS, it may be taken to represent the ratio of S_{tt}/S_{tot} . However, this is valid under the assumption that the density of di-8-ANEPPS labelling per unit of membrane area was uniform over peripheral and TATS membrane compartments. The average “volume ratio” derived by Gorelik et al. was 0.728 for control myocytes, which is the highest estimate either published or computed on the basis of the present study. This ratio dropped to an average of 0.432 after detubulation. Assuming that S_{surf} did not change, we computed that 34% of the initial S_{tt} would remain after detubulation. See section 4.4 for further discussion.

3.3. Comparison of estimates from morphological measurements to simulated values

When the weight of the animals was given, we plotted the values of the S_{tt}/S_{tot} fraction as derived in section 3.2 (Table 1) versus the myocyte volume of the central point of the artificial data series that corresponded to their weight class. These appear in Fig. 2 as grey-filled symbols of the same type as the series corresponding to the rat weight reported by the authors. For convenience, these data have been overshadowed in grey colour in Table 1 and numbers from the first column of Table 1 were added near the symbols in Fig. 2. The values for Sprague-Dawley rats appear in Fig. 2A. The large open symbols number 9 and 10 correspond to the study of Satoh et al. (1996). Our simulations overestimated the corresponding S_{tt}/S_{tot} values of Table 1. This might be due to some inadequacy of the shape of a rod with elliptic cross-section that we chose. Although our computations were adjusted to correctly estimate the rendered volumes evaluated by Satoh et al. (1996), they may have underestimated the surface area of the myocytes. Our corrections for membrane infolding, caveolae and intercalated disk complexity may also need to be adjusted. Among studies on 200 g rats, studies (1), (4), (5) and (7) on Sprague-Dawley rats and (3), unidentified strain from Page and McCallister (1973a), are in reasonable match with our simulations. It should be noted that Page and co-workers, in studies (1), (5), (6) and (7) used Sprague-Dawley rats, which may apply for study (3). Study (12), on ~300 g rats, shows a value sizeably lower than our simulation for 250 g rats. Study (6) on 300 g rats falls well below our simulations for 250 g (open triangles) or ~350 g rats (open squares). Study (14) is consistent with the highest weight class (open circles) of ~496 g rats and with study (10). As a whole, our simulations might be revised to better account for values from the literature on Sprague-Dawley rats, namely studies (9) and (10), which we took as a basis. In panel B of Fig. 2, we plotted the S_{tt}/S_{tot} values from Wistar rats. The upper value from study (2) and the value from study (8), for 200 g rats, are much higher than our simulation (open diamonds). The lower value from study (2) may be considered as consistent, as would both values from study (11) for 250 g rats. Study (13) is consistent with our simulation for ~350 g rats but was done on 300 g rats.

As a whole, the S_{tt}/S_{tot} values from morphological studies on both rat strains confirm a trend to increase with myocyte volume, as related to increasing body weight.

3.4. Comparing estimates of the TATS membrane fraction using morphological analysis versus C_m analysis with formamide detubulation

In order to compare all studies of Tables 1 and 2, we gathered the data on two graphs in Fig. 3. Comparing the estimates from morphological studies (Table 1 S_{tt}/S_{tot} values converted in %) with those based on formamide detubulation (Table 2), Fig. 3A shows a general underestimation by the latter, that holds when considering either Sprague-Dawley rats (lozenges) or Wistar rats (circles), whereas values for unidentified rat strains (triangles) are similar. For all studies specifying the weight of the rats, the S_{tt}/S_{tot} data from Table 1 were plotted in % versus weight in Fig. 3B. Data from studies

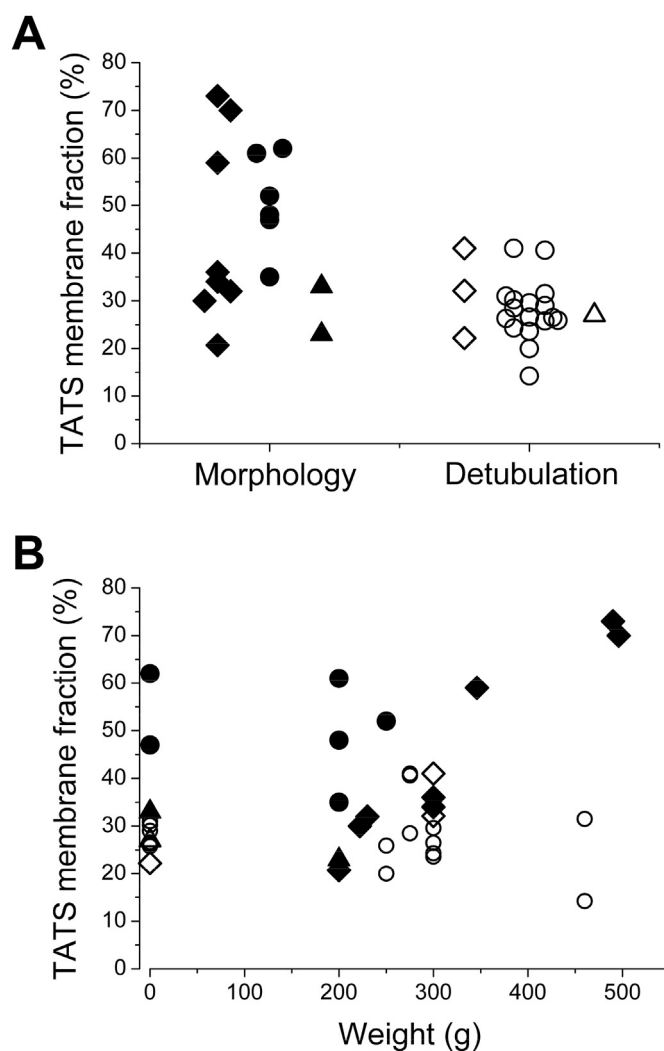


Fig. 3. Values of the TATS membrane fraction as evaluated from morphological studies (filled symbols, Table 1) or detubulation studies (open symbols, Table 2) in Sprague-Dawley rats (lozenges), Wistar rats (circles) or rats of unspecified strain (triangles). Values the TATS membrane fraction (S_{tt}/S_{tot}) from Table 1 were expressed in %, instead of fraction, to allow comparison with data from Tab.2. In A, all values were plotted for each of the two methods. The three series of data were offset horizontally for clarity. A further variable horizontal offset was applied to the symbols within a given series, for clarity. In B, values were plotted versus weight. When not available, weight was defaulted to zero.

that did not specify body weight were plotted on the left vertical axis. The data from detubulation studies in Wistar rats (open circles in Fig. 3B) include 9 data points within 250–300 g weights and two data points at 460 g. The outlying data from Gadeberg et al. (2016) showing a TATS membrane fraction of 14.2% ought to be disregarded, since it is more than two times lower than the value resulting from a parallel study (Bryant et al., 2015) on the same animals (see Table 2). The dispersion of the 10 remaining data points precludes any global visual relationship. Eight data points from morphological studies on Sprague-Dawley rats seem to indicate a positive correlation of TATS membrane fraction with weight. This is further analysed in section 4.3.

From the 20 reported measurements of loss of capacitance upon formamide detubulation of all studies on rat ventricular myocytes (Table 2), an average value of 28.5% is computed for the TATS membrane fraction. Taking into account that, on average, detubulated myocytes still have about 8% of their TATS area remaining connected to the outside (Pasek et al., 2008a), or up to 16% (Bryant et al., 2015), we attempted to correct for the effect of a f_{tres} value at 0.16 and computed values "% C_m lost corr." in Table 2. We omitted the outlying value from Gadeberg et al. (2016), see above. The average corrected value of TATS membrane fraction of the remaining studies is at 35.7%. It is at 35.3% when considering only male Wistar rats. This would still be in the lower range of values from morphological studies at comparable body weights. Taking into account an average myocyte C_m of 143 pF and a C_m/V_{myo} of 5.4 pF/pL (for 300 g rats), V_{myo} ought to be 26.5 pL (Fig. 1C, open triangles). The TATS membrane fraction value corresponding to this volume in our simulation in Fig. 2 for a 300 g rat is 0.53. Thus, the TATS membrane fraction estimated from detubulation, even after correcting for incomplete detubulation, is sizeably lower than the expected values from our simulations and from morphological measurements (Table 1).

4. Discussion

4.1. Myocyte dimensions and shape

For their computations of myocyte volume, Boyett et al. (1991) used a rod with an elliptical cross section with a 1/3 ratio of width to thickness (Sorenson et al., 1985). The data in Table 1 of Satoh et al. (1996) for rat myocytes show a ratio at 2.41 ± 0.65 (we estimated the error of 0.65 after summing relative errors in width and depth). From Table 2 of Satoh et al. (1996) we computed width to thickness ratios of 2.63 in adolescent rats and 2.42 in adult rats. In our simulated data sets, we generated a set of values with the same relative 95% confidence interval as the data of Satoh et al. in 6 months rats. It turns out that the width to thickness ratio varies between 2 and 2.7, the lower values being for smaller myocytes. This is consistent with the observation that myocytes from smaller animals tend to be less flattened (Sorenson et al., 1985). It appears that we chose the upper limit in setting the width to thickness to 3.0. In further simulations, we ought to adjust this parameter to a consensual value at 2.5 and possibly make it depend on myocyte length or age.

As to the length to width (l/w) ratio, the present synthetic data sets have l/w ratios spanning 3.4 to 5.7 and show a decrease when myocyte size increases. The following l/w values may be computed from published data in rat ventricular myocytes: 4.5 in rats of either sex 250–300 g (Boyett et al., 1991); 5.03 in adult male Sprague-Dawley rats 250–350 g (Stimers and Dobretsov, 1998); 3.5 in female adult Wistar rats (Kawai et al., 1999); 5.02 in male Wistar rats (Brette et al., 2000); 3.85 in control and 3.08 in hypertrophied right ventricular myocytes from adult male Sprague-Dawley rats of 350–400 g (Chouabe et al., 1997); from 3.76 to 4.54 in control (380–495 g) and 2.78 to 3.81 in hypertrophied myocytes from adult male Sprague-Dawley rats, with differences according to region in

the left ventricle (Benitah et al., 1993). At change, Satoh et al. (1996) measured averaged length to width ratios of 4.19 and 3.7 in 6 months (~500 g) and 3 months (~350 g) rats respectively. Thus the span of l/w ratios in our synthetic data set is consistent with ratios computed from published values and their changes along rat weight. Also of note, myocyte dimensions and l/w ratios did not differ among three rat strains at 3 months age, spontaneously hypertensive (SHR), Wistar-Kyoto (WKY) and Fischer-344 rats, managed and studied in the same laboratory (Bishop et al., 1979), so we did not seek to explain discrepancies as resulting from morphological differences between rat strains.

4.2. The lower size limit for TATS morphogenesis

Using electron microscopy, a lower limit of 7–8 μm in myocyte diameter has been measured for rat ventricular myocytes to have a TATS (Hirakow, 1970). In living rat atrial myocytes under confocal microscopy, this limit appears between 11.7 and 13.2 μm (Kirk et al., 2003). These two ranges of values come into agreement when considering a 45% myocyte shrinkage upon preparation for electron microscopy (Eisenberg and Mobley, 1975). In the present simulations, the peripheral membrane area to myocyte volume ratio increased when the size of a rod shape with elliptic cross section was decreased (Fig. 1A), so that, for a myocyte width of 12.9 μm , the upper limit of the whole membrane area to volume ratio of $6.76 \mu\text{m}^2/\mu\text{m}^3$ in 3-months-rats was attained. Under the assumption that the amount of TATS is governed by this constraint, there would be no need for a 12 μm wide myocyte of developing a TATS in the present synthetic data series. Thus the hypothesis of a constraint for a minimal membrane area to volume ratio could be enough to explain that the smaller atrial myocytes and yet smaller myocytes in the AV-node and SA-node are devoid of TATS (Brette et al., 2002). However, myocytes from very young rats having myocyte diameters as low as 7.8 μm may still have a $S_{\text{tt}}/S_{\text{tot}}$ of 13% (Stewart and Page, 1978), pointing to a different determinism of the TATS in ventricular versus atrial or nodal cells.

4.3. Dependence of $S_{\text{tt}}/S_{\text{tot}}$ on rat weight

The data generated in this study also account for the progressive increase in the amount of TATS as is evidenced in the EM micrographs of Nakamura et al. (1986) taken from the ventricle of 28 g up to 490–560 g Wistar rats in 7 different classes of weights and in the data of Stewart and Page (1978) for Sprague-Dawley rats 44.5–300 g body weight, yielding TATS membrane fractions increasing from 13% to about 35% respectively. Furthermore, the apparently high membrane fraction in TATS derived from the analysis of Soeller and Cannell (1999) for 250 g Wistar rats turns out to be in agreement with the data of Satoh et al. (1996) and with our simulation (Fig. 2B, study (11)) once plausible corrections were applied. The large value derived by Gorelik et al. (2006) by computing the ratio of TATS-related fluorescence to total fluorescence in a confocal slice is likely an overestimate, as discussed in 4.4.

It appeared in Fig. 2A that TATS membrane fraction data from morphological studies in Sprague-Dawley rats (filled lozenges) might indicate a correlation with body weight. A linear regression analysis is depicted in Fig. 4. Despite considering a reasonable 20% relative standard deviation in both TATS membrane fraction and weight data, a tight correlation was found. The fitted line intercept value at $-10.4 \pm 17.5\%$ cannot be considered as different from zero. The slope was estimated at $0.167 \pm 0.065\%/g$ with a low relative error. Thus, TATS membrane fraction may be considered as increasing proportionally to body weight. Of note, the TATS membrane fraction values read along the fitted line are 23% at 200 g and 31% at 250 g body weight whereas in our simulations (Fig. 2) they are 26% and 46%

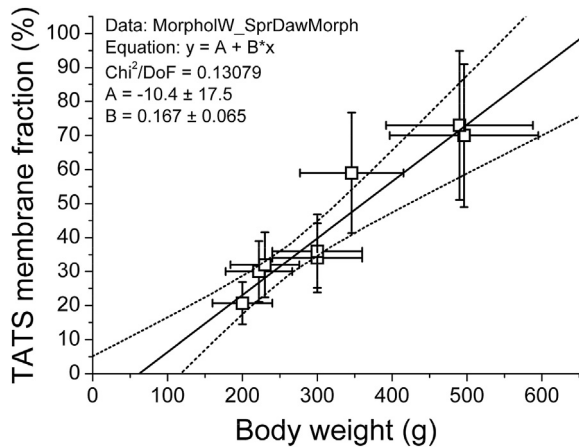


Fig. 4. Relationship of the membrane fraction in TATS S_{tt}/S_{tot} (expressed in %) with body weight, as determined from morphological studies in Sprague-Dawley rat myocardium (Table 1). Open squares report the mean TATS membrane fraction versus mean weight values. A uniform relative standard deviation of 0.2 was assumed for both body weight and TATS membrane fraction measurements (respectively s_{xi} and s_{yi}) and are reported as error bars. Weighting of the fit included both errors in the form: $w_i = 1/((B \cdot s_{xi})^2 + s_{yi}^2)$. The solid line equation was $y = A + B \cdot x$ with $A = -10.4 \pm 17.5\%$ and $B = 0.167 \pm 0.065\%/g$. The dashed lines show the upper and lower 95% confidence limits. The calculation of Pearson's correlation coefficient R was omitted because it neglects any error associated with the mean values.

respectively. Values at 346 and 496 g are 48% and 72.6% respectively versus 63% and 73% respectively in our simulation. This confirms that our simulations need adjustment to match the experimental data. Regarding data from Wistar rats in Fig. 3B, no such correlation was attempted from morphological data, since only 4 values are available and two of them are in contradiction. From detubulation studies, the outlier point from Gadeberg et al. (2016) being excluded, a single point remains outside of a cluster of points spanning a narrow weight range (250–300 g). This is not surprising, because detubulation studies aimed at deriving data on the distribution of ion channels in standard conditions and mostly used young adults.

4.4. Comparability of morphological and detubulation estimates of S_{tt}/S_{tot}

Overestimation of S_{tt}/S_{tot} might result from a slow internalisation of di-8-ANEPPS with time into the sarcoplasm (Chaloupka et al., 1997) unduly counted as tubular membrane fluorescence. However, this possibility was ruled out by Soeller and Cannell (1999). Another possible bias could arise if a single confocal slice was analysed in each myocyte and would be at the mid-height of a myocyte lying flat. Referring to the transverse sections shown in Fig. 6 of Soeller and Cannell (1999) one may observe that this would maximize the volume of the slice and thereby the amount of TATS. In addition, the density of the TATS is maximal at mid-height. This would also minimize the area of peripheral membrane since most of the surface membrane will be oriented perpendicular to the plane of the confocal slice. In comparison, in a confocal slice nearing the upper or lower boundaries of the myocyte, the surface membrane plane will be obliquely oriented and will contribute a larger part of the fluorescence signal, whereas the density of the TATS will be lower. The integrative 3D analyses of Satoh et al. (1996) and of Soeller and Cannell (1999) take all of the internal voxels into account, which avoids such drawbacks.

Thomas et al. (2003) reported complete detubulation while most other studies have evaluated a fraction of TATS resisting detubulation (non-detubulated and incompletely detubulated myocytes) from 8% (Pasek et al., 2008a) to 16% (Bryant et al. (2015) whereas we

evaluated a high value at 36% from Gorelik et al.'s (2006) data. There could be an opportunity to improve the efficiency of formamide detubulation if the reasons of the full detubulation by Thomas et al. were deciphered. A possible explanation for a fraction of intact t-tubules remaining could be a partial protection of the TATS by small permeant molecules (Uchida et al., 2016).

When comparing the formamide detubulation procedure with that induced by imipramine, Bourcier et al. (2019) reported a decay of 45% of rod-shaped myocytes in male Wistar rats' ventricular myocytes upon formamide detubulation. If this decay would preferentially affect larger cells, the remaining myocytes would have lower TATS membrane fraction values, which might explain why Thomas et al. (2003) observed a low-range average TATS membrane fraction at 26.5% although all of their rod-shaped myocytes, after formamide treatment, appeared completely detubulated. Further, Bourcier et al. (2019) evaluated a TATS membrane fraction of 40% comparing imipramine-detubulated myocytes to control ones. This value is only at the higher range found from formamide-detubulation studies. Thus, inconvenients of the formamide detubulation revealed by the imipramine method did not resolve the discrepancy with morphological methods. Correcting the ensemble of data from detubulation studies for incomplete detubulation did not succeed either (see 3.4). This suggests that morphological studies did overestimate the TATS membrane fraction. One possible reason analysed by Pasek et al. (2008a) was the possibility that the specific capacitance of the TATS membrane might be lower than that of the surface membrane, due to a higher content in cholesterol. However, a recent study by Gadeberg et al. (2017) did not reveal a change in C_m/V_{myo} of mouse ventricular myocytes upon cholesterol depletion using methyl- β -cyclodextrin. This does not preclude another unknown reason for the specific membrane capacitance to be different in surface and tubular membranes.

4.5. Limitations

In this study, we referred to body weight and/or age of the animals, which may be confusing. The authors had preferred to be able to refer to one single parameter, i.e.: weight, because a larger body weight imposes an increased workload to the heart, causing physiological hypertrophy at any age. Likewise, animal strain and gender are important parameters, and we did not attempt to consider possible differences. However, it readily appears from Table 1 that among 14 studies, eight of them omitted to specify either age (8) or body weight (1) or both (1). This also goes for omitting gender (4) or rat strain (2), and one study reported using male and female rats. Similarly, in Table 2, over 18 studies, age is omitted in 12 of them, body-weight in 7 and gender in 8. As a whole, methods have been under documented, which hinders attempts to figure out the influence of some parameters and provides sense to the "Minimum Information about a Cardiac Electrophysiology Experiment (MICCE)" initiative (Quinn et al., 2011). Whenever willing to translate from age to weight, we might refer to the values of ages and weights reported by Nakamura et al. (1986) for Wistar rats as plotted in Fig. 5. They show a proportional relationship from 1 week to 6 months with an increment of about 30 g/week. The data from Wistar rats (open circles) below 500 g agree well with Nakamura's data. The data from Sprague-Dawley rats of Satoh et al. (1996) at 3 months (~350 g) agree with that relationship, as do those of Despa et al. (2003) and Garcarena et al. (2013) at 300 g. Data for ages around 6 months (25–27 weeks) from Wistar or Sprague-Dawley rats depart from the linear relation. Other studies in Table 2 reported age or weight or none, and the term "adult Wistar" was used for rats having weights ranging 250–300 g with two exceptions at 450 and 460 g.

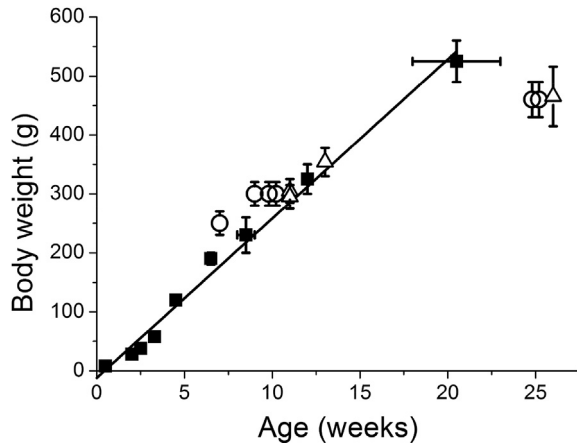


Fig. 5. Weights and ages of Wistar rats were collected from the detailed study of Nakamura et al. (1986) and their relationship was plotted (filled squares), with error bars reporting the span of weights and/or age, when present. The regression line indicates proportionality with a slope of about 30 g/week. Open circles show the data for Wistar rats in Tables 1 and 2. Open triangles report the data for Sprague-Dawley rats. When not reported, a putative 10% dispersion of the weight was associated with open symbols.

In generating our datasets, it was assumed that myocyte width and depth changed in parallel to myocyte length and that the statistical dispersion of values in these three dimensions was principally due to differences in myocyte length. However, it was reported that the individual length to width ratio of ventricular myocytes of the rabbit ranged from 2.16 to 7.4 (Taniguchi et al., 1981). This suggests that there is a large independent variation of length and width of the myocytes, and that shorter myocytes do not necessarily have smaller widths. In this respect, the span of myocyte volumes in our synthetic data series may be exaggerated.

It was shown that ventricular myocytes from adult rats appeared binucleated for 85% of them and 15% mononucleated. The mean length and width were significantly larger in binucleated myocytes and the volume was doubled, versus mononucleated ones (Bishop et al., 1979). This was neglected by Satoh et al. (1996) and may contribute to increase the dispersion around the mean dimensions of the myocytes. Thus, accounting for two separate populations should be more accurate, not only for simulating, but perhaps also for analysing data from a population of rat ventricular myocytes.

An assumption in extrapolating to rats of lower weight classes (200 and 250 g) was that average myocyte dimensions would increase linearly with animal weight and that relative dispersion would remain constant. This is in agreement with a linear increase of myocyte length with body weight in Sprague-Dawley rats from 45 to 200 g of $\sim 20 \mu\text{m/g}$ (Stewart and Page, 1978).

It was assumed that the amount of TATS would ensure a constant area to volume ratio, however, the amount of TATS differs along the long axis of the myocyte, as it is larger at mid length of the myocyte than at its ends (Mitcheson et al., 1996; Quinn et al., 2003). Thus the amount of TATS may rather be correlated with local width as shown in mouse atrial myocytes (Yue et al., 2017).

Our assumption of a direct proportionality of C_m to V_{myo} within one class of weights cannot be directly supported by Fig. 4B of Satoh et al. (1996) because they analysed the relation of V_{myo} to C_m . However, we have read data out from Fig. 4B of Satoh et al. and performed a linear regression of C_m to V_{myo} resulting in the relation: $C_m = (7.5 \pm 1.4) * V_{\text{myo}} + (33 \pm 51)$ (not shown). The large value of the error on the intercept at $V_{\text{myo}} = 0$ suggests that C_m is not different from zero at this point. Given the low relative error on the slope, we may assume that C_m was proportional to V_{myo} .

4.6. Determinants of TATS development

Two functional requirements are in line with a constant area to volume ratio. The need to synchronize Ca release and hence contraction requires conduction of the excitation instantaneously to the whole myocyte volume, a function which is ensured by the voltage homogeneity of cardiac TATS membrane beyond micro-seconds after a voltage change, as evaluated in computer models of rat and guinea-pig ventricular myocytes (Pasek et al., 2006, 2008b, 2008c), in agreement with subcellular voltage sensitive dye measurements (Windisch et al., 1995; Sacconi et al., 2012), which was also confirmed by Scardigli et al. (2017) using FRAP microscopy. Furthermore, couplings of the membrane with the SR (dyads) ought to be present at short distance from the contractile material, to avoid diffusion delay from the periphery to contractile units, this would require extension of the TATS to the centre of the myocyte. Metabolic supply in states of high demand requires transfer of glucose to the myocyte interior. GLUT4 transporters are translocated both at peripheral and at TATS membranes under stimulation by insulin alone (Retz et al., 1996) or associated with exercise (Slot et al., 1991). Therefore, the maximal glucose transfer rate to the myocyte ought to be proportional to the total membrane area. This shall also be true for ion transfer by mechanisms that are more evenly distributed, especially for the Na-K pump or the Na-Ca exchanger that regulate intracellular ion homeostasis. Molecular mechanisms that trigger and regulate the morphogenesis of TATS and its association with ion channels, receptors and effectors are being progressively deciphered as reviewed e.g. by Ibrahim et al. (2011) and Hong and Shaw (2017).

4.7. Proper statistical distributions of biophysical parameters of cardiac myocytes

The values of measurements done on single cardiac myocytes such as morphological and electrical parameters are generally assumed to be pseudo-Gaussian, so that computations of average, standard deviation and standard error on the mean use the canonical formulas of Gaussian statistics. However, almost all of these parameters are strictly positive quantities that may even have a sizeable minimal plausible value. These features apply to measured values of the capacitance of isolated rat ventricular cardiac myocytes. The Gaussian distribution, when the ratio of SD to mean is small, is deemed an acceptable approximation allowing statistical comparisons of experimental data series. However, when using Monte-Carlo simulations, creating artificial data series as Gaussian random numbers, we noted that unrealistic small (or even negative) values appeared, which compromised the statistical behaviour of the whole series. The Log-Gaussian distribution ensures that no values at or lower than zero can be generated, further, it behaves as Gaussian if the logarithm of the variable is considered, thus still allowing usual statistical comparisons (Limpert et al., 2001; Limpert and Stahel, 2011).

4.8. Statistical errors and their propagation in TATS membrane fraction determination

In most studies using detubulation to evaluate TATS membrane fraction, two sub-populations are separated from a unique pool of isolated myocytes, one of which remains intact while the other is subjected to detubulation. Assuming perfect detubulation, C_m values are measured from a sample of n_i and n_d myocytes in each sub-population and the mean values (C_{mi} and C_{md}), each associated with its own standard deviation (sd_i and sd_d) are used to compute the quantity $a = (C_{mi} - C_{md}) / C_{mi}$. To evaluate the final standard deviation, absolute errors sum up for a subtraction and relative errors

sum up for a division. Since $C_{mi}-C_{md}$ will be at least 2 fold smaller than either C_{md} or C_{mi} , the final relative error on the TATS membrane fraction is currently 3- to 4- fold larger than those of C_{mi} and C_{md} alone. When this further combines with ionic current values in order to evaluate current densities in surface and TATS membranes, average currents I_i in intact myocytes and I_d in detubulated ones are combined to provide $b=(I_i-I_d)/I_d$ the fraction of current in the TATS and b/a is then the current density in the TATS. When considering the mean values, if a large number of myocytes is studied, the central limit theorem tells us that the mean values will be well estimated, but the error will remain large and this will hinder conclusions about the statistical significance of the differences observed. An aggravating condition, as confirmed by the present study, is that a large part of the variability in C_m values is not due to random myocyte to myocyte variations, but C_{mi} depends on the size of the myocyte, and further, the TATS membrane fraction value does as well. One ideal way to circumvent these drawbacks would be to have each myocyte acting as its own control, and it is expected that the number of experiments to achieve a given level of significance of the differences might be affordable. It was proven possible to maintain a myocyte in conditions of whole-cell patch-clamp throughout the detubulation procedure (Kawai et al., 1999). This approach will require that the detubulation occurs soon enough to allow measurements being made before and after detubulation, and also that the measurement procedure be repeatable. For example, if imipramine-induced detubulation (Bourcier et al., 2019) is applicable in a few minutes and remains stable, it might be an alternative. Another possibility, within the separate populations of myocytes, would be to use myocytes of comparable size, thus eliminating the size-related variability, and for so doing, it might be preferable to pre-select myocytes having similar volumes, which can be evaluated with some precision using the projected area, since it was shown to be almost linearly related to myocyte volume (Satoh et al., 1996). In any case, such possibilities may well be simulated using our framework, once adjusted to closely represent the features of the myocytes from a given strain/species and a given age/weight class. This could help optimising a chosen strategy, or choosing among possible strategies to achieve a given goal in significance.

4.9. Applicability and relevance of our proposal

The underlying assumption that the amount of TATS in a myocyte is increased so as to keep the myocyte membrane area to myocyte volume constant may apply to physiological rat hearts (Satoh et al., 1996), to myocyte hypertrophy due to thyroxin exposure (McCallister and Page, 1973; Page and McCallister, 1973a) or due to exercise in mouse hearts (Stolen et al., 2009) in which TATS density was kept constant while myocyte volume increased. However this does not necessarily apply to hypertrophy seen in pathological states where TATS may decrease or remain constant but changes shape or is disorganised (Seidel et al., 2017; Louch et al., 2010).

Our study has disclosed that the framework has to be adjusted to age/weight of the animals, to account for a particular set of myocytes. Application to the analysis of sets of myocytes from diseased regions of the myocardium might reveal a loss of inner linkages between biophysical parameters e.g.: TATS amount and myocyte size, suggesting that a regulatory mechanism is disrupted. Our approach may be applied to generate separate sets of cardiac myocytes with different inner linkages, which might perhaps help deciphering whether a mixture of two types of myocytes may account for an unaccountable apparent dispersion. It also could be used to generate subsets of myocytes corresponding to different regions, with different morphologies, electrophysiological

properties or different inner TATS structures as in Colli-Franzone et al. (2006). Interestingly, a variable TATS distribution has recently been quantified in rat and pig atria as a decreasing transmural gradient from epicardium to endocardium, for which a role in synchronisation of contraction of the atrial wall was deciphered from mathematical modelling (Frisk et al., 2014). These authors also report three types of myocytes in rat atria: untubulated, tubulated and organized-tubulated while a single type of ventricular myocytes is found. A tight link of amplitude of the calcium current to myocyte capacitance and to C_m/V_{myo} is also revealed. The same group disclosed a difference in TATS amount between myocytes from the base and the apex in rat and mouse ventricles (Wright et al., 2018). Models of cardiac myocytes with different properties are generated to account for the behaviour of different populations of myocytes as to the state of their TATS, owing to heart failure (Loucks et al., 2018). These are approaches similar to ours in which once there are defined, for each subgroup, the myocyte parameters, the shape of their statistical distribution and the links between parameters, then realistic populations of myocytes can be generated and the behaviour of their combination into 3D tissue structures can be compared to that of uniform structures. Finally, our approach may well be combined with any detailed electro-ionic model of single myocytes, e.g.: (Livshitz et al., 2012), since only features at the whole myocyte level are generated in our approach.

5. Conclusions

The proposed framework reasonably agrees with published data documenting the relations of TATS membrane fraction to myocyte volume within several classes of body weights. It provides a basis for analysing the sources of imprecision in the evaluation of the areas of TATS and surface membrane and their related ionic current densities. As a result, strategies are suggested for minimizing the influence of non-random data dispersion of TATS membrane fraction related to myocyte volume. The framework described in this work might serve to generate large sets of artificial isolated myocyte populations adapted to age and myocyte sizes, with realistic features, links between parameters and constrained statistical distributions. The next step is to use such datasets to evaluate the improvement of measurements depending on sample size, dependencies, biases and errors.

CRediT authorship contribution statement

Georges Christé: Conceptualization, Formal analysis, Software, Visualization, Writing - original draft, Writing - review & editing. **Robert Bonvallet:** Supervision, Methodology. **Christophe Chouabe:** Conceptualization, Formal analysis, Writing - review & editing.

Declaration of competing interest

None.

Appendix

This section explains the bases for our computation and how we conducted them.

6.1 Myocyte dimensions

It is intuitive that the peripheral area to volume ratio of an object keeping constant shape shall decrease as its volume increases, since volume increases faster than peripheral area. However, to obtain a quantitative representation of this phenomenon in cardiac

myocytes, a suitable morphological model has to be designed. Ventricular cardiac myocytes resemble rods with a rather short outfit. In vertical projection, their aspect is almost rectangular with partial spindle-like narrowing towards its ends and irregularities in width. Models used by various experimenters to estimate myocyte volume from the measured length and width (and sometimes depth) have differed in the shape of the cross section: rectangular (parallelepiped), circular (cylinder), ellipsoid with rectangular vertical projection or spindle-like with circular or ellipsoid cross-section. These models have been compared by [Satoh et al. \(1996\)](#) for the ability of the volumes (computed using measured length, width and depth) to account for 3D-rendered volume analysed from confocal imaging of freshly dissociated myocytes. The rendered volume was 0.54 times that of the parallelepiped, 1.42 times that of the spindle but 0.71 times that of the rod with ellipsoid cross section ([Satoh et al., 1996](#)). In the present development, the myocyte was assumed to have an elongated rod-like shape with ellipsoid cross section with a ratio of thickness to width of about 1/3 ([Sorenson et al., 1985](#); [Boyett et al., 1991](#)). Myocyte dimensions were assumed to have negligible measurement error (an absolute error of $\pm 0.5 \mu\text{m}$ seems an acceptable assumption). The cell-to-cell dispersion of length values around the mean was consensually reported by authors with mean \pm SD (or sem and n) as if it would follow a normal distribution. A series of equally spaced length values was generated, spanning the interval mean -SD to mean +SD. An odd number of values were generated, so that the mean value would be represented as the central value.

The ratio of myocyte length to myocyte width is preserved across myocyte sizes in rat left ventricular myocytes ([Bishop and Drummond, 1979](#)). The ratio of myocyte thickness to myocyte width may be considered as constant ([Sorenson et al., 1985](#); [Boyett et al., 1991](#)). Thus, myocyte width and thickness were assumed to be linear functions of myocyte length within ventricular myocytes from rats of a given weight and were computed so that their values span the mean -SD to mean +SD interval of measurements by [Satoh et al. \(1996\)](#).

The general formula was

$$w = (l - l_{\text{mean}}) / SD_l * SD_w + w_{\text{mean}} \text{ (in } \mu\text{m)} \quad (\text{A1})$$

$$\text{th} = (l - l_{\text{mean}}) / SD_l * SD_{\text{th}} + \text{th}_{\text{mean}} \text{ (in } \mu\text{m)} \quad (\text{A2})$$

thus, for 6 months rats:

$$w = (l - 140.1) / 16.4 * 4.8 + 33.4 \text{ (in } \mu\text{m)} \text{ and} \quad (\text{A3})$$

$$\text{th} = (l - 140.1) / 16.4 * 1.5 + 13.8 \text{ (in } \mu\text{m)}; \quad (\text{A4})$$

and for 3 months rats:

$$w = (l - 123.8) / 14.4 * 6.7 + 33.6 \text{ (in } \mu\text{m)} \text{ and} \quad (\text{A5})$$

$$\text{th} = (l - 123.8) / 14.4 * 1.4 + 12.8 \text{ (in } \mu\text{m)}. \quad (\text{A6})$$

The perimeter of the elliptic cross section was computed using an approximate formula:

$$\text{peri} = \pi * \text{sqrt} [2 * (a^2 + b^2) - (a - b)^2 / 2] \text{ with } a = w/2 \text{ and } b = \text{th}/2 \quad (\text{A7})$$

(<http://www.numericana.com/answer/ellipse.htm>) that has a relative precision of about $4 * 10^{-13}$.

$$S_{\text{end}} = \pi * w * \text{th} / 4 \quad (\text{A8})$$

(in μm^2) is the area of the intercalated disks at one end of the

myocyte;

$$S_{\text{long}} = \text{peri} * l \quad (\text{A9})$$

(in μm^2) is the side area of the myocyte (excluding intercalated disks);

$$S_{\text{surf}} = S_{\text{long}} + S_{\text{end}} * 2 \quad (\text{A10})$$

(in μm^2) is the total myocyte surface area;

$$V_{\text{myo}} = S_{\text{end}} * l \quad (\text{A11})$$

(in μm^3) is the myocyte volume.

6.2 Extrapolation to lower rat weights

Myocyte length is in approximate linear relation with weight ([Stewart and Page, 1978](#)) and the ratio of myocyte length to myocyte width is almost constant ([Sorenson et al., 1985](#)). Therefore putative theoretical mean values of myocyte length (l_{mean}), width (w_{mean}) and thickness (th_{mean}) were extrapolated from 6 months rat data (496 g) down to weights (W) of 250 and 200 g, using:

$$l_{\text{mean}} = (140.1 - 123.8) / (496 - 346) * (W - 346) + 123.8 \quad (\text{A12})$$

$$w_{\text{mean}} = 33.6 / (496) * (W - 346) + 33.6 \quad (\text{A13})$$

$$\text{th}_{\text{mean}} = 13.8 / (496) * (W - 346) + 13.8 \quad (\text{A14})$$

It was assumed that the relative dispersion (SD/mean) of each variable was constant across rat weights, the SD value of each variable corresponding to rat weights of 200 and 250 g was computed from its measured values at 6 months to be proportional to the above computed mean value.

A series of values were generated as a set of 9 or 11 regularly spaced values of length, spanning the range ($l_{\text{mean}} - \text{SD}$) to ($l_{\text{mean}} + \text{SD}$), where SD is the standard deviation. Series of values for myocyte width and thickness were generated for each rat weights of 200 and 250 g with formulas (for the case of extrapolating to 200 g rat weight from 6 months rats), the indexes "200" and "6mo" mean 200 g and 6 months respectively:

$$w = (l - l_{\text{mean}}) * (SD_{w200}) / (SD_{w6mo}) + w_{\text{mean}} \quad (\text{A15})$$

$$\text{th} = (l - l_{\text{mean}}) * (SD_{\text{th}200}) / (SD_{\text{th}6mo}) + \text{th}_{\text{mean}} \quad (\text{A16})$$

6.3 Correction for the presence of caveolae

It has been measured in rabbit papillary muscle that caveolae augment plasmalemmal area by 21–32%, assuming two or three caveolae per neck, respectively ([Levin and Page, 1980](#)). This is true for peripheral and TATS membranes. [Page \(1978\)](#) showed that in rabbit papillary muscle the caveolar plasma membrane contributed 14–21% to the total plasmalemma with no significant difference between the tubular system and external sarcolemma. Rat myocytes have more caveolae necks than rabbit and extended branched chains of caveolae were observed in rats ([Severs et al., 1982](#)). Thus 21% is likely to be in the lower range of realistic values for the rat. The correction factor for caveolae is thus 1.21.

6.4 Computing the increase in membrane area due to membrane infolding

Peripheral membrane presents sizeable infolding that is readily visible in scanning EM microscopy (Nag et al., 1977; Nag and Zak, 1979) and was termed Z-folds (Severs et al., 1985). Scanning ion conductance microscopy (SICM) has been used to confirm and further characterize this infolding in freshly dissociated rat ventricular myocytes that was defined as 'Z-grooves' (Gorelik et al., 2006).

Assuming that the profile of the transverse section of the peripheral membrane through Z-grooves profile is a succession of half ellipses (Gorelik et al., 2006) with a and b being the short and long radii, then the ratio of the ellipsoid profile to the linear one is:

$$\begin{aligned} \text{profile length} &= \pi * \text{sqrt} [2 * (a^2 + b^2) - (a-b)^2 / 2] / \\ 2 &= 2.0563 \mu\text{m}, \end{aligned} \quad (\text{A17})$$

where $a = 0.35 \mu\text{m}$ and $b = 0.9 \mu\text{m}$. The flat profile length is $1.8 \mu\text{m}$, thus the increase in profile length is by a factor $2.0563 / 1.8 = 1.1424$ at the level of Z-grooves. Thus, the overall factor taking into account the Z-groove factor is:

$$((1-Z) + Z * 1.1424) = 1.12. \quad (\text{A18})$$

This factor should only apply to peripheral membrane excluding the intercalated disks (see below).

The membrane area due to infolding and to caveolae is included into the measured myocyte capacitance. It is not included when peripheral membrane area is computed from myocyte shape, or when tubular membrane area is estimated from the smoothed profile of TATS in electron microscopy or confocal microscopy. It was thus needed to correct morphological estimates of the peripheral membrane area by a factor of $1.12 + 0.21$, i.e. 1.33 that corrected altogether for caveolae and infolding and that of TATS membrane area for caveolae only, i.e.: by a factor of 1.21.

6.5 Effect of membrane infolding and caveolae on measured myocyte volume

Neglecting infolding and caveolae might misestimate myocyte volume but this ought not to be significant since caveolae have a very large area to volume ratio and since alternating gain and loss of small volumes across the mid-profile through membrane infolding likely cancelled each other.

6.6 Intercalated disk area

There is considerable infolding of myocyte membrane at the level of the intercalated disk, which increases membrane area by 2.3 fold from a flat plane through the intercalated disk (Hoyt et al., 1989). The area of membrane at the myocyte endings (i.e.: twice the cross section area) represents about 6% of the total peripheral membrane area. No correction for caveolae was applied to this area.

Whenever the peripheral membrane area measurement has been reported as a whole, we applied the above assumption. The overall correcting factor for the increase in peripheral membrane area due to caveolae, membrane infolding and intercalated disk indentations is then: $0.06 * 2.3 + (1-0.06) * 1.33 = 1.39$. The correction factor for TATS membrane area includes caveolae only and amounts to 1.21.

6.7 Specific membrane capacitance

Gentet et al. (2000) found a specific capacitance of $0.9 \mu\text{F}/\text{cm}^2$ in several types of neurons. This is not influenced by the amount of

exogenously expressed protein. Likewise, Gilai (1976) found values of 0.90 and $0.91 \mu\text{F}/\text{cm}^2$ respectively for surface and for tubular membrane of skeletal muscle fibres. Consequently, the true specific capacitance ought to be lower than the canonical value of $1 \mu\text{F}/\text{cm}^2$. Thus, a value of $0.9 \mu\text{F}/\text{cm}^2$ may be regarded as an upper limit of the real specific capacitance. This value was used to translate capacitance into membrane area. The canonical value of $1 \mu\text{F}/\text{cm}^2$ was also used to allow comparisons with the literature that mostly used this value.

6.8 Corrections to myocyte volume: rendering factor

Whenever volumes computed from the idealized shape of myocytes ought to be compared to 3D-rendered volumes estimated from confocal images of real myocytes, they were corrected for the discrepancy of the rendered volume to the geometrical computation of myocyte volume as was estimated by Satoh et al. (1996).

When mean values for myocyte length, width and thickness in Table 2 of Satoh et al. (1996) are used to compute the volume of a rod-shaped myocyte with elliptic cross section, volumes of $41818 \mu\text{m}^3$ and $50717 \mu\text{m}^3$ are found for average myocytes of 3 months old rats and 6 months old rats respectively. These volumes translate to 41.8 and 50.7 pL respectively, whereas mean rendered volumes in Satoh et al. (1996) were 30.9 and 36.8 pL respectively. Thus the correction factor is respectively 0.74 and 0.73 . This indicates that the correction factor did not differ significantly between the two ages. However, they noted that the shape of cardiac ventricular myocytes was more indented in older animals. Therefore, the correction factor was assumed to be higher for 250 g (0.80) and 200 g rats (0.90). We used these values to translate computed volumes into rendered volumes at different ages.

6.9 Peripheral area to volume ratio

Peripheral myocyte area was computed as corresponding to a rod-shaped myocyte with ellipsoidal cross section (Sorenson et al., 1985; Boyett et al., 1991). However, it was estimated by Satoh et al. (1996) that the volume estimated from 3D volume rendering was 29% smaller than that of a rod-shaped myocyte with ellipsoidal cross-section, which they attributed to uneven width of the myocyte along its long axis. In such a case, the projected area of the real myocyte would also be about 29% smaller than the projection area of the idealized rod shaped myocyte evaluated as the product of length by width. It is supported by the finding of Satoh et al. that rendered volume is proportional to this product (length by depth) (their Fig. 4A). This is approximately the case within our synthetic datasets (Fig. 1B). Therefore, myocyte peripheral area would be overestimated by the same fraction as myocyte volume in the present computations, so that the peripheral area to volume ratio computed for a rod with elliptic cross section should be equivalent to the area to volume ratio of the real myocyte.

6.10 Capacitance to volume ratio at low weights

The smallest myocyte in a 200 g rat in our synthetic data series (ellipsoidal section-rod shaped myocyte with length $80 \mu\text{m}$, width $14 \mu\text{m}$, thickness $7.2 \mu\text{m}$) has an uncorrected computed peripheral area to volume ratio of $0.45 \mu\text{m}^2/\mu\text{m}^3$, which translates to $4.5 \text{ pF}/\text{pL}$ assuming $1 \mu\text{F}/\text{cm}^2$ as specific capacitance (or $4.05 \text{ pF}/\text{pL}$ assuming $0.9 \mu\text{F}/\text{cm}^2$). If now applying corrections with an infolding factor of 1.12 and caveolae factor of 1.21, this ratio is $0.644 \mu\text{m}^2/\mu\text{m}^3$, which translates to $6.44 \text{ pF}/\text{pL}$ (or $5.8 \text{ pF}/\text{pL}$ with $0.9 \mu\text{F}/\text{cm}^2$). Thus, within the assumption that the linear relation of total membrane area to myocyte volume ratio also applies to myocytes of animals younger than those studied by Satoh et al. (1996), the total membrane area

to volume ratio is likely to reach a minimal value that is determined by the maximal peripheral membrane area to volume ratio attained for the smallest myocytes. Therefore, it was assumed that the constant area to volume ratio for 200 and 250 g rats was the same as for 3 months rats, i.e. $0.676 \mu\text{m}^2/\mu\text{m}^3$, which translates to 6.76 pF/pL with $1 \mu\text{F}/\text{cm}^2$ or 6.08 pF/pL with $0.9 \mu\text{F}/\text{cm}^2$.

6.11 Converting capacitance to volume ratio into area to volume ratio

The conversion of the measured total myocyte capacitance to volume ratio (k_c in pF/pL) into area to volume ratio (k_a in $\mu\text{m}^2/\mu\text{m}^3$), assuming that the peripheral and TATS membranes have the same specific capacitance (sc in $\mu\text{F}/\text{cm}^2$) is done using:

$$k_a = k_c / sc * 10^{-1} (\mu\text{m}^2/\mu\text{m}^3) \quad (\text{A19})$$

6.12 Fraction of membrane in the TATS

If $S_{\text{surf}}/V_{\text{myo}}$ is the computed peripheral membrane area to myocyte volume ratio, then the TATS membrane area to myocyte volume ratio is given by:

$$S_{\text{tt}}/V_{\text{myo}} = S_{\text{tot}}/V_{\text{myo}} - S_{\text{surf}}/V_{\text{myo}} (\mu\text{m}^2/\mu\text{m}^3) \quad (\text{A20})$$

This expresses the hypothesis that TATS morphogenesis obeys the constraint of maintaining a constant membrane area to volume ratio.

The fraction of myocyte membrane located in the TATS is computed as:

$$S_{\text{tt}}/S_{\text{tot}} = S_{\text{tt}}/V_{\text{myo}} / (S_{\text{tot}}/V_{\text{myo}}) (\text{dimensionless}) \quad (\text{A21})$$

References

Benitah, J.P., Gomez, A.M., Bailly, P., Da Ponte, J.P., Berson, G., Delgado, C., Lorente, P., 1993. Heterogeneity of the early outward current in ventricular cells isolated from normal and hypertrophied rat hearts. *J. Physiol.* 469, 111–138.

Bishop, S.P., Oparil, S., Reynolds, R.H., Drummond, J.L., 1979. Regional myocyte size in normotensive and spontaneously hypertensive rats. *Hypertension* 1, 378–383.

Bishop, S.P., Drummond, J.L., 1979. Surface morphology and cell size measurement of isolated rat cardiac myocytes. *J. Mol. Cell. Cardiol.* 11, 423–433.

Bourcier, A., Barthe, M., Bedioune, I., Lechene, P., Miled, H.B., Vandecasteele, G., Fischmeister, R., Leroy, J., 2019. Imipramine as an alternative to formamide to detubulate rat ventricular cardiomyocytes. *Exp. Physiol.* 104, 1237–1249.

Boyett, M.R., Frampton, J.E., Kirby, M.S., 1991. The length, width and volume of isolated rat and ferret ventricular myocytes during twitch contractions and changes in osmotic strength. *Exp. Physiol.* 76, 259–270.

Brette, F., Calaghan, S.C., Lappin, S., White, E., Colyer, J., Le Guennec, J.Y., 2000. Biphasic effects of hyposmotic challenge on excitation-contraction coupling in rat ventricular myocytes. *Am. J. Physiol.* 279, H1963–H1971.

Brette, F., Komukai, K., Orchard, C.H., 2002. Validation of formamide as a detubulation agent in isolated rat cardiac cells. *Am. J. Physiol.* 283, H1720–H1728.

Brette, F., Salle, L., Orchard, C.H., 2004a. Differential modulation of L-type Ca^{2+} current by SR Ca^{2+} release at the T-tubules and surface membrane of rat ventricular myocytes. *Circ. Res.* 95, e1–e7.

Brette, F., Rodriguez, P., Komukai, K., Colyer, J., Orchard, C.H., 2004b. Beta-adrenergic stimulation restores the Ca transient of ventricular myocytes lacking t-tubules. *J. Mol. Cell. Cardiol.* 36, 265–275.

Brette, F., Salle, L., Orchard, C.H., 2006. Quantification of calcium entry at the T-tubules and surface membrane in rat ventricular myocytes. *Biophys. J.* 90, 381–389.

Brette, F., Orchard, C.H., 2006a. Density and sub-cellular distribution of cardiac and neuronal sodium channel isoforms in rat ventricular myocytes. *Biochem. Biophys. Res. Commun.* 348, 1163–1166.

Brette, F., Orchard, C.H., 2006b. No apparent requirement for neuronal sodium channels in excitation-contraction coupling in rat ventricular myocytes. *Circ. Res.* 98, 667–674.

Bryant, S., Kimura, T.E., Kong, C.H., Watson, J.J., Chase, A., Suleiman, M.S., James, A.F., Orchard, C.H., 2014. Stimulation of ICa by basal PKA activity is facilitated by caveolin-3 in cardiac ventricular myocytes. *J. Mol. Cell. Cardiol.* 68, 47–55.

Bryant, S.M., Kong, C.H., Watson, J., Cannell, M.B., James, A.F., Orchard, C.H., 2015. Altered distribution of ICa impairs Ca release at the t-tubules of ventricular myocytes from failing hearts. *J. Mol. Cell. Cardiol.* 86, 23–31.

Chaloupka, R., Plasek, J., Slavik, J., Siglerova, V., Sigler, K., 1997. Measurement of membrane potential in *Saccharomyces cerevisiae* by the electrochromic probe di-4-ANEPPS: effect of intracellular probe distribution. *Folia Microbiol.* 42, 451–456.

Chase, A., Colyer, J., Orchard, C.H., 2010. Localised Ca channel phosphorylation modulates the distribution of L-type Ca current in cardiac myocytes. *J. Mol. Cell. Cardiol.* 49, 121–131.

Chouabe, C., Espinosa, L., Megas, P., Chakir, A., Rougier, O., Freminet, A., Bonvallet, R., 1997. Reduction of I(Ca,L) and I(to1) density in hypertrophied right ventricular cells by simulated high altitude in adult rats. *J. Mol. Cell. Cardiol.* 29, 193–206.

Colli-Franzone, P., Pavarino, L.F., Taccardi, B., 2006. Effects of transmural electrical heterogeneities and electrotonic interactions on the dispersion of cardiac repolarization and action potential duration: a simulation study. *Math. Biosci.* 204, 132–165.

Despa, S., Brette, F., Orchard, C.H., Bers, D.M., 2003. Na/Ca exchange and Na/K-ATPase function are equally concentrated in transverse tubules of rat ventricular myocytes. *Biophys. J.* 85, 3388–3396.

Despa, S., Bers, D.M., 2007. Functional analysis of Na+/K+-ATPase isoform distribution in rat ventricular myocytes. *Am. J. Physiol.* 293, C321–C327.

Duclohier, H., 2005. Neuronal sodium channels in ventricular heart cells are localized near T-tubules openings. *Biochem. Biophys. Res. Commun.* 334, 1135–1140.

Eisenberg, B.R., Mobley, B.A., 1975. Size changes in single muscle fibers during fixation and embedding. *Tissue Cell* 7, 383–387.

Frisk, M., Koivumaki, J.T., Norseng, P.A., Maleckar, M.M., Sejersted, O.M., Louch, W.E., 2014. Variable t-tubule organization and Ca^{2+} homeostasis across the atria. *Am. J. Physiol. Heart Circ. Physiol.* 307, H609–H620.

Gadeberg, H.C., Bryant, S.M., James, A.F., Orchard, C.H., 2016. Altered Na/Ca exchange distribution in ventricular myocytes from failing hearts. *Am. J. Physiol. Heart Circ. Physiol.* 310, H262–H268.

Gadeberg, H.C., Kong, C.H.T., Bryant, S.M., James, A.F., Orchard, C.H., 2017. Cholesterol depletion does not alter the capacitance or Ca handling of the surface or t-tubule membranes in mouse ventricular myocytes. *Phys. Rep.* 5, 5–22.

Garciaarena, C.D., Ma, Y.L., Swietach, P., Huc, L., Vaughan-Jones, R.D., 2013. Sarcolemmal localisation of Na^+/H^+ exchange and $\text{Na}^+/\text{HCO}_3^-$ co-transport influences the spatial regulation of intracellular pH in rat ventricular myocytes. *J. Physiol.* 591, 2287–2306.

Genet, L.J., Stuart, G.J., Clements, J.D., 2000. Direct measurement of specific membrane capacitance in neurons. *Biophys. J.* 79, 314–320.

Gilai, A., 1976. Electromechanical coupling in tubular muscle fibers. II. Resistance and capacitance of one transverse tubule. *J. Gen. Physiol.* 67, 343–367.

Gorelik, J., Yang, L.Q., Zhang, Y., Lab, M., Korchev, Y., Harding, S.E., 2006. A novel Z-groove index characterizing myocardial surface structure. *Cardiovasc. Res.* 72, 422–429.

Hirakow, R., 1970. Ultrastructural characteristics of the mammalian and sauropsidan heart. *Am. J. Cardiol.* 25, 195–203.

Hong, T.T., Shaw, R.M., 2017. Cardiac t-tubule microanatomy and function. *Physiol. Rev.* 97, 227–252.

Hoyt, R.H., Cohen, M.L., Saffitz, J.E., 1989. Distribution and three-dimensional structure of intercellular junctions in canine myocardium. *Circ. Res.* 64, 563–574.

Ibrahim, M., Gorelik, J., Yacoub, M.H., Terracciano, C.M., 2011. The structure and function of cardiac t-tubules in health and disease. *Proc. Biol. Sci.* 278, 2714–2723.

Kawai, M., Hussain, M., Orchard, C.H., 1999. Excitation-contraction coupling in rat ventricular myocytes after formamide-induced detubulation. *Am. Heart J.* 277, H603–H609.

Kirk, M.M., Izu, L.T., Chen-Izu, Y., McCulle, S.L., Wier, W.G., Balke, C.W., Shorofsky, S.R., 2003. Role of the transverse-axial tubule system in generating calcium sparks and calcium transients in rat atrial myocytes. *J. Physiol.* 547 (2), 441–451.

Komukai, K., Brette, F., Yamanashi, T.T., Orchard, C.H., 2002. K(+) current distribution in rat sub-epicardial ventricular myocytes. *Pflügers Archiv* 444, 532–538.

Leeson, T.S., 1978. The transverse tubular (T) system of rat cardiac muscle fibers as demonstrated by tannic acid mordanting. *Can. J. Zool.* 56, 1906–1916.

Leeson, T.S., 1980. T-tubules, couplings and myofibrillar arrangements in rat atrial myocardium. *Acta Anat.* 108, 374–388.

Levin, K.R., Page, E., 1980. Quantitative studies on plasmalemmal folds and caveolae of rabbit ventricular myocardial cells. *Circ. Res.* 46, 244–255.

Lewis, C.J., Gong, H., Brown, M.J., Harding, S.E., 2004. Overexpression of beta 1-adrenoceptors in adult rat ventricular myocytes enhances CGP 12177A cardiostimulation: implications for 'putative' beta 4-adrenoceptor pharmacology. *Br. J. Pharmacol.* 141, 813–824.

Limpert, E., Stahel, W.A., Abbt, M., 2001. Log-normal distributions across the sciences: keys and clues. *Bioscience* 51, 341–352.

Limpert, E., Stahel, W.A., 2011. Problems with using the normal distribution-and ways to improve quality and efficiency of data analysis. *PLoS One* 6, e21403.

Livshitz, L., Acsai, K., Antoons, G., Sipido, K., Rudy, Y., 2012. Data-based theoretical identification of subcellular calcium compartments and estimation of calcium

- dynamics in cardiac myocytes. *J. Physiol.* 590, 4423–4446.
- Louch, W.E., Sejersted, O.M., Swift, F., 2010. There goes the neighborhood: pathological alterations in T-tubule morphology and consequences for cardiomyocyte Ca^{2+} handling. *J. Biomed. Biotechnol.* 2010, 503906. Epub 2010 Apr 8, 503906.
- Loucks, A.D., O'Hara, T., Trayanova, N.A., 2018. Degradation of T-tubular microdomains and altered cAMP compartmentation lead to emergence of arrhythmic triggers in heart failure myocytes: an in silico study. *Front. Physiol.* 9, 1737. <https://doi.org/10.3389/fphys.2018.01737> eCollection@2018., 1737.
- McCallister, L.P., Page, E., 1973. Effects of thyroxin on ultrastructure of rat myocardial cells: stereological study. *J. Ultrastruct. Res.* 42, 136–155.
- Mitcheson, J.S., Hancox, J.C., Levi, A.J., 1996. Action potentials, ion channel currents and transverse tubule density in adult rabbit ventricular myocytes maintained for 6 days in cell culture. *Pflügers Archiv* 431, 814–827.
- Nag, A.C., Fischman, D.A., Aumont, M.C., Zak, R., 1977. Studies of isolated adult rat heart cells: the surface morphology and the influence of extracellular calcium ion concentration on cellular viability. *Tissue Cell* 9, 419–436.
- Nag, A.C., Zak, R., 1979. Dissociation of adult mammalian heart into single cell suspension: an ultrastructural study. *J. Anat.* 129, 541–559.
- Nakamura, S., Asai, J., Hama, K., 1986. The transverse tubular system of rat myocardium: its morphology and morphometry in the developing and adult animal. *Anat. Embryol.* 173, 307–315.
- Page, E., McCallister, L.P., Power, B., 1971. Stereological measurements of cardiac ultrastructures implicated in excitation-contraction coupling. *Proc. Natl. Acad. Sci. U. S. A* 68, 1465–1466.
- Page, E., McCallister, L.P., 1973b. Studies on the intercalated disk of rat left ventricular myocardial cells. *J. Ultrastruct. Res.* 43, 388–411.
- Page, E., McCallister, L.P., 1973a. Quantitative electron microscopic description of heart muscle cells: application to normal, hypertrophied and thyroxin treated hearts. *Am. J. Cardiol.* 31, 172–181.
- Page, E., 1978. Quantitative ultrastructural analysis in cardiac membrane physiology. *Am. J. Physiol.* 235, C147–C158.
- Page, E., Surdyk-Droske, M., 1979. Distribution, surface density, and membrane area of diadic junctional contacts between plasma membrane and terminal cisterns in mammalian ventricle. *Circ. Res.* 45, 260–267.
- Pager, J., 1971. Etude morphométrique du système tubulaire transverse du myocarde ventriculaire de rat. *J. Cell Biol.* 50, 233–237.
- Pasek, M., Simurda, J., Christé, G., 2006. The functional role of cardiac T-tubules explored in a model of rat ventricular myocytes. *Philos. Transact. A Math. Phys. Eng. Sci.* 364, 1187–1206.
- Pasek, M., Brette, F., Nelson, D.A., Pearce, C., Qaiser, A., Christé, G., Orchard, C.H., 2008a. Quantification of T-tubule area and protein distribution in rat cardiac ventricular myocytes. *Prog. Biophys. Mol. Biol.* 96/1–3, 244–257.
- Pasek, M., Simurda, J., Orchard, C.H., Christé, G., 2008b. A model of the Guinea-pig ventricular cardiomyocyte incorporating a transverse-axial tubular system. *Prog. Biophys. Mol. Biol.* 96/1–3, 258–280.
- Pasek, M., Simurda, J., Christé, G., Orchard, C.H., 2008c. Modelling the cardiac transverse-axial tubular system. *Prog. Biophys. Mol. Biol.* 96/1–3, 226–243.
- Pasek, M., Simurda, J., Christé, G., 2017. Different densities of Na-Ca exchange current in t-tubular and surface membranes and their impact on cellular activity in a model of rat ventricular cardiomyocyte. *BioMed Res. Int.* 2017, 6343821.
- Quinn, F.R., Currie, S., Duncan, A.M., Miller, S., Sayeed, R., Cobbe, S.M., Smith, G.L., 2003. Myocardial infarction causes increased expression but decreased activity of the myocardial $\text{Na}^{+}\text{-Ca}^{2+}$ exchanger in the rabbit. *J. Physiol.* 553, 229–242.
- Quinn, T.A., Granite, S., Alessie, M.A., Antzelevitch, C., Bollensdorff, C., Bub, G., Burton, R.A., Cerbai, E., Chen, P.S., Delmar, M., DiFrancesco, D., Earm, Y.E., Efimov, I.R., Egger, M., Entcheva, E., Fink, M., Fischmeister, R., Franz, M.R., Garny, A., Giles, W.R., Hanes, T., Harding, S.E., Hunter, P.J., Iribe, G., Jalife, J., Johnson, C.R., Kass, R.S., Kodama, I., Koren, G., Lord, P., Markhasin, V.S., Matsuoka, S., McCulloch, A.D., Mirams, G.R., Morley, G.E., Nattel, S., Noble, D., Olesen, S.P., Panfilov, A.V., Trayanova, N.A., Ravens, U., Richard, S., Rosenbaum, D.S., Rudy, Y., Sachs, F., Sachse, F.B., Saint, D.A., Schotten, U., Solovoyova, O., Taggart, P., Tung, L., Varro, A., Volders, P.G., Wang, K., Weiss, J.N., Wettwer, E., White, E., Wilders, R., Winslow, R.L., Kohl, P., 2011. Minimum Information about a Cardiac Electrophysiology Experiment (MICEE): standardised reporting for model reproducibility, interoperability, and data sharing. *Prog. Biophys. Mol. Biol.* 107, 4–10.
- Rett, K., Wicklmayr, M., Dietze, G.J., Haring, H.U., 1996. Insulin-induced glucose transporter (GLUT1 and GLUT4) translocation in cardiac muscle tissue is mimicked by bradykinin. *Diabetes* 45, S66–S69.
- Sacconi, L., Ferrantini, C., Lotti, J., Coppini, R., Yan, P., Loew, L.M., Tesi, C., Cerbai, E., Poggesi, C., Pavone, F.S., 2012. Action potential propagation in transverse-axial tubular system is impaired in heart failure. *Proc. Natl. Acad. Sci. U. S. A* 109, 5815–5819.
- Satoh, H., Delbridge, L.M.D., Blatter, L.A., Bers, D.M., 1996. Surface:volume relationship in cardiac myocytes studied with confocal microscopy and membrane capacitance measurements: species-dependence and developmental effects. *Biophys. J.* 70, 1494–1504.
- Scardigli, M., Crocini, C., Ferrantini, C., Gabbriellini, T., Silvestri, L., Coppini, R., Tesi, C., Rog-Zielinska, E.A., Kohl, P., Cerbai, E., Poggesi, C., Pavone, F.S., Sacconi, L., 2017. Quantitative assessment of passive electrical properties of the cardiac T-tubular system by FRAP microscopy. *Proc. Natl. Acad. Sci. U. S. A* 114, 5737–5742.
- Seidel, T., Navankasattusas, S., Ahmad, A., Diakos, N.A., Xu, W.D., Tristani-Firouzi, M., Bonios, M.J., Taleb, I., Li, D.Y., Selzman, C.H., Drakos, S.G., Sachse, F.B., 2017. Sheet-like remodeling of the transverse tubular system in human heart failure impairs excitation-contraction coupling and functional recovery by mechanical unloading. *Circulation* 135, 1632–1645.
- Severs, N.J., Slade, A.M., Powell, T., Twist, V.W., Warren, R.L., 1982. Correlation of ultrastructure and function in calcium-tolerant myocytes isolated from the adult rat heart. *J. Ultrastruct. Res.* 81, 222–239.
- Severs, N.J., Slade, A.M., Powell, T., Twist, V.W., Jones, G.E., 1985. Morphometric analysis of the isolated calcium-tolerant cardiac myocyte. Organelle volumes, sarcomere length, plasma membrane surface folds, and intramembrane particle density and distribution. *Cell Tissue Res.* 240, 159–168.
- Slot, J.W., Geuze, H.J., Gigengack, S., James, D.E., Lienhard, G.E., 1991. Translocation of the glucose transporter GLUT4 in cardiac myocytes of the rat. *Proc. Natl. Acad. Sci. U. S. A* 88, 7815–7819.
- Soeller, C., Cannell, M.B., 1999. Examination of the transverse tubular system in living cardiac rat myocytes by 2-photon microscopy and digital image-processing techniques. *Circ. Res.* 84, 266–275.
- Sorenson, A.L., Tepper, D., Sonnenblick, E.H., Robinson, T.F., Capasso, J.M., 1985. Size and shape of enzymatically isolated ventricular myocytes from rat and cardiomyopathic hamsters. *Cardiovasc. Res.* 19, 793–799.
- Stewart, J.M., Page, E., 1978. Improved stereological techniques for studying myocardial cell growth: application to external sarcolemma, T system, and intercalated disks of rabbit and rat hearts. *J. Ultrastruct. Res.* 65, 119–134.
- Stimers, J.R., Dobretsov, M., 1998. Adrenergic stimulation of Na/K pump current in adult rat cardiac myocytes in short-term culture. *J. Membr. Biol.* 163, 205–216.
- Stolen, T.O., Hoydal, M.A., Kemi, O.J., Catalucci, D., Ceci, M., Aasum, E., Larsen, T., Rolim, N., Condorelli, G., Smith, G.L., Wisloff, U., 2009. Interval training normalizes cardiomyocyte function, diastolic Ca^{2+} control, and SR Ca^{2+} release synchronicity in a mouse model of diabetic cardiomyopathy. *Circ. Res.* 105, 527–536.
- Swift, F., Stromme, T.A., Amundsen, B., Sejersted, O.M., Sjaastad, I., 2006. Slow diffusion of K^{+} in the T tubules of rat cardiomyocytes. *J. Appl. Physiol.* 101, 1170–1176.
- Swift, F., Tovsrud, N., Enger, U.H., Sjaastad, I., Sejersted, O.M., 2007. The $\text{Na}^{+}/\text{K}^{+}$ -ATPase α 2-isoform regulates cardiac contractility in rat cardiomyocytes. *Cardiovasc. Res.* 75, 109–117.
- Swift, F., Birkeland, J.A., Tovsrud, N., Enger, U.H., Aronsen, J.M., Louch, W.E., Sjaastad, I., Sejersted, O.M., 2008. Altered $\text{Na}^{+}/\text{Ca}^{2+}$ -exchanger activity due to downregulation of $\text{Na}^{+}/\text{K}^{+}$ -ATPase α 2-isoform in heart failure. *Cardiovasc. Res.* 78, 71–78.
- Taniguchi, J., Kokubun, S., Noma, A., Irisawa, H., 1981. Spontaneously active cells isolated from the sino-atrial and atrio-ventricular nodes of the rabbit heart. *Jpn. J. Physiol.* 31, 547–558.
- Thomas, M.J., Sjaastad, I., Andersen, K., Helm, P.J., Wasserstrom, J.A., Sejersted, O.M., Ottersen, O.P., 2003. Localization and function of the $\text{Na}^{+}/\text{Ca}^{2+}$ exchanger in normal and detubulated rat cardiomyocytes. *J. Mol. Cell. Cardiol.* 35, 1325–1337.
- Uchida, K., Moench, I., Tamkus, G., Lopatin, A.N., 2016. Small membrane permeable molecules protect against osmotically induced sealing of t-tubules in mouse ventricular myocytes. *Am. J. Physiol. Heart Circ. Physiol.* 311, H229–H238.
- Windisch, H., Ahammer, H., Schaffer, P., Muller, W., Platzer, D., 1995. Optical multisite monitoring of cell excitation phenomena in isolated cardiomyocytes. *Pflügers Archiv* 430, 508–518.
- Wright, P.T., Bhogal, N.K., Diakonov, I., Pannell, L.M.K., Perera, R.K., Bork, N.J., Schobesberger, S., Lucarelli, C., Faggian, G., Alvarez-Laviada, A., Zaccolo, M., Kamp, T.J., Balijepalli, R.C., Lyon, A.R., Harding, S.E., Nikolaev, V.O., Gorelik, J., 2018. Cardiomyocyte membrane structure and cAMP compartmentation produce anatomical variation in beta2AR-cAMP responsiveness in murine hearts. *Cell Rep.* 23, 459–469.
- Yang, Z., Pascarel, C., Steele, D.S., Komukai, K., Brette, F., Orchard, C.H., 2002. $\text{Na}^{+}/\text{Ca}^{2+}$ exchange activity is localized in the T-tubules of rat ventricular myocytes. *Circ. Res.* 91, 315–322.
- Yao, A., Spitzer, K.W., Ito, N., Zaniboni, M., Lorell, B.H., Barry, W.H., 1997. The restriction of diffusion of cations at the external surface of cardiac myocytes varies between species. *Cell Calcium* 22, 431–438.
- Yue, X., Zhang, R., Kim, B., Ma, A., Philipson, K.D., Goldhaber, J.I., 2017. Heterogeneity of transverse-axial tubule system in mouse atria: remodeling in atrial-specific $\text{Na}^{+}/\text{Ca}^{2+}$ exchanger knockout mice. *J. Mol. Cell. Cardiol.* 108, 50–60. <https://doi.org/10.1016/j.yjmcc.2017.05.008>. Epub@2017 May@19, 50–60.